ARTICLE

Homeostatic circuits selectively gate food cue responses in insular cortex

Yoav Livneh[1], Rohan N. Ramesh[1,2], Christian R. Burgess[1], Kirsten M. Levandowski[1], Joseph C. Madara[1], Henning Fenselau[1], Glenn J. Goldey[1], Veronica E. Diaz[1], Nick Jikomes[1,2], Jon M. Resch[1], Bradford B. Lowell[1,2]§ & Mark L. Andermann[1,2]§

Physiological needs bias perception and attention to relevant sensory cues. This process is 'hijacked' by drug addiction, causing cue-induced cravings and relapse. Similarly, its dysregulation contributes to failed diets, obesity, and eating disorders. Neuroimaging studies in humans have implicated insular cortex in these phenomena. However, it remains unclear how 'cognitive' cortical representations of motivationally relevant cues are biased by subcortical circuits that drive specific motivational states. Here we develop a microprism-based cellular imaging approach to monitor visual cue responses in the insular cortex of behaving mice across hunger states. Insular cortex neurons demonstrate food-cue-biased responses that are abolished during satiety. Unexpectedly, while multiple satiety-related visceral signals converge in insular cortex, chemogenetic activation of hypothalamic 'hunger neurons' (expressing agouti-related peptide (AgRP)) bypasses these signals to restore hunger-like response patterns in insular cortex. Circuit mapping and pathway-specific manipulations uncover a pathway from AgRP neurons to insular cortex via the paraventricular thalamus and basolateral amygdala. These results reveal a neural basis for state-specific biased processing of motivationally relevant cues.

The needs of the body focus attention on sensory cues associated with outcomes that can satisfy these needs. Dysregulation of this process contributes to pathological conditions including obesity, eating disorders, and addiction. Human neuroimaging studies suggest that insular cortex (InsCtx) plays a key role in these phenomena[1,2]. Indeed, InsCtx integrates interoceptive signals from throughout the body with taste information[3–5]. To begin to explore how physiological needs influence InsCtx, we investigated the role of hunger in InsCtx processing of learned food-predicting cues.

Hunger-dependent increases in visual food cue responses in human InsCtx are associated with increased incentive value[1,6]. In obesity and eating disorders, elevated responses persist after satiation[7,8]. Rodent InsCtx neurons respond to learned cues[9–12], and InsCtx is required for food cues to elicit behavioural responses[10,13]. However, the mechanisms by which motivation-related subcortical circuits drive this process remain unknown.

Here we develop a novel approach for cellular-resolution imaging of InsCtx in behaving mice across hunger and satiety, combined with circuit mapping and pathway-specific manipulations. We uncover a specific pathway from hunger-related AgRP neurons[14,15] to InsCtx, via the paraventricular thalamus (PVT) and basolateral amygdala (BLA). Our findings provide a framework for explorations of how natural and pathological need states converge in InsCtx to bias behavioural responses towards relevant cues.

Imaging InsCtx activity in behaving mice

We trained food-restricted mice to perform a go/no-go visual discrimination task in which licking after different learned visual cues led to delivery of liquid food (Ensure), aversive bitter solution (quinine), or no outcome[16] (Fig. 1a). After performance during hunger, mice consumed unlimited quantities of Ensure to satiety (operationally defined as voluntary cessation of consumption; ~3–5 ml, ~30–75 min). Subsequent food-cue-evoked licking was greatly reduced (Fig. 1b and Extended Data Fig. 1a).

We first asked whether InsCtx is necessary for performance of this operant task. Pharmacological silencing of InsCtx, but not of adjacent secondary somatosensory cortex, reliably and reversibly impaired performance by reducing responses to food cues, without affecting responses to other cues or locomotion (Fig. 1c and Extended Data Fig. 1b–d). Despite encompassing primary visceral and gustatory cortices[17], InsCtx was not required for home-cage feeding on chow (Fig. 1d), nor for *ad libitum* Ensure consumption in the task apparatus but in the absence of visual cues (Fig. 1e). Thus, InsCtx is important for operant behavioural responses to learned food-predicting cues (Supplementary Discussion).

InsCtx has been inaccessible to imaging in behaving animals because of its deep and lateral location behind essential skull and jaw bones[18,19]. We developed a novel preparation that spared these bones, using a reflective microprism[20]. Intact InsCtx was thus imaged without anaesthesia or head rotation[18,19]. We combined this approach with viral expression of GCaMP6f to simultaneously image the activity of 150–200 neurons in superficial layers of InsCtx in behaving mice (Fig. 1f, Extended Data Fig. 2a and Supplementary Video).

Many InsCtx neurons responded to the food cue, licking, Ensure[4,12,21], or both the food cue and licking/Ensure (Fig. 1g). The sign (excitation/suppression) of these responses was uncorrelated (cue-licking: $r = 0.01$, $P = 0.8$; cue-Ensure: $r = -0.1$, $P = 0.07$; Extended Data Fig. 2b). Remarkably, 88% of neurons responded to the food cue and/or feeding (828 out of 941 neurons, six mice; Fig. 1h). A large subset (~30%) responded to the visual food cue, of which 85% also responded to licking/Ensure, suggesting that InsCtx food cue responses may represent predictions about gustatory and interoceptive consequences of upcoming consumption (Fig. 1h).

We next examined the spatial functional organization of InsCtx[5,18,19]. InsCtx was previously reported to contain a topographic map of gustatory features in naive, anaesthetized mice[19]. However, we did not observe any large-scale (hundreds of micrometres) or fine-scale (tens of micrometres) organization of neurons responding to the food cue or to

---

[1]Division of Endocrinology, Diabetes and Metabolism, Beth Israel Deaconess Medical Center, Harvard Medical School, Boston, Massachusetts 02215, USA. [2]Program in Neuroscience, Harvard Medical School, Boston, Massachusetts 02115, USA.
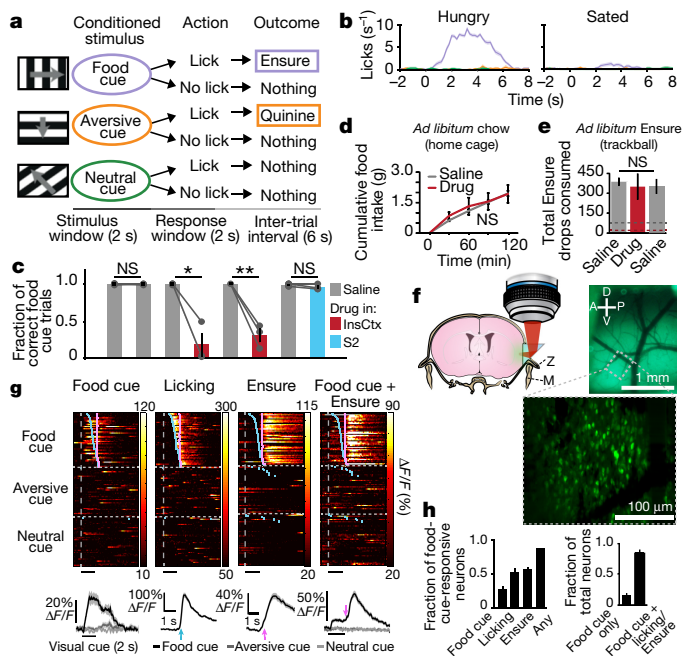§These authors jointly supervised this work.

Figure 1 | Chronic imaging of InsCtx activity during an InsCtx-dependent behavioural task. a, Visual discrimination task. **b**, Example task performance, across hunger and satiety. Mean ± s.e.m. **c**, Task performance. Lines connect within-session blocks. Mean ± s.e.m.; NS, $P \geq 0.2$; *$P = 0.03$; **$P = 0.01$; paired t-test, $n = 3$ mice. S2, secondary somatosensory cortex. **d**, Home-cage chow consumption. NS, $P \geq 0.14$; paired t-test, $n = 4$ mice. Mean ± s.e.m. **e**, *Ad libitum* Ensure consumption. NS, $P \geq 0.38$; paired t-test, $n = 3$ mice. Dashed lines: average consumption during the task in **c**. Mean ± s.e.m. **f**, Coronal section illustrating the microprism imaging approach with intact skull (Z, zygomatic) and jaw (M, mandible) bones. Top right: epifluorescence image through the microprism of InsCtx surface vasculature. D, dorsal; A, anterior; P, posterior; V, ventral. Bottom: two-photon image. **g**, Example single neurons with responses to different events. Top: heatmaps. Rows: single trials sorted by lick-bout onset (blue ticks). Magenta ticks: Ensure delivery. Bottom: average responses. **h**, Left: fraction of neurons ($n = 941$) responsive to different events. Right: fraction of food-cue-responsive neurons ($n = 274$) also responsive to licking and/or Ensure. Mean ± s.e.m. across six mice.

licking/Ensure. Additionally, while previous work suggested functional differences between granular and dysgranular subregions of InsCtx[3], we did not observe any (Extended Data Fig. 2c–g). Thus, in behaving mice, the cellular representation of food cues and subsequent food consumption is dense and spatially distributed throughout InsCtx.

Hunger gates InsCtx cue responses

We next considered the effects of homeostatic state on InsCtx cue responses by imaging the same neurons across hunger and satiety (Fig. 2a). Strikingly, the average population response across neurons excited (red) or suppressed (blue) by visual cues during hunger was abolished during satiety (Fig. 2b). During hunger, neurons were three times more likely to respond to the food cue than to others, and food-cue-responsive neurons rarely responded to other cues (Fig. 2c and d, left, middle). Responses were largest to food cues, intermediate to avoidable aversive cues, and smallest to neutral cues. Satiation eliminated the food cue bias by differentially attenuating food cue responses (Fig. 2c and d, right). These effects were more prominent in neurons excited compared with those suppressed by cues (Extended Data Fig. 3a–d). Cue responses did not show systematic attenuation across a session, although trial-to-trial response variability was higher than in visual cortical areas[16] (Extended Data Fig. 3e, f). We calculated a 'hunger modulation index' (Fig. 2e), which revealed stronger responses during

hunger versus satiety in 89% of neurons (244 out of 274). Thus, most InsCtx neurons showed selective responses to the food cue, which were attenuated during satiety.

Food cue bias was due to motivational salience rather than to inherent visual biases or overexposure to food cues early in training (Methods): cue responses in untrained, hungry mice were weaker, less prevalent, and not food cue-biased[9] (Extended Data Fig. 3g), and InsCtx food cue bias was similar before and after switching the visual stimuli associated with food and neutral outcomes (Extended Data Fig. 3h–m). Further, while orofacial movements can modulate InsCtx activity[4,21], these were unlikely to underlie food cue bias or hunger modulation (Extended Data Fig. 4a, b). Indeed, using simultaneous orofacial videography[9] and InsCtx imaging, we found that food cue responses were only positively correlated with preparatory orofacial movements in 3% of neurons (Extended Data Fig. 4c–g and Supplementary Discussion).

Neurons in Fig. 2 were selected on the basis of responsiveness during hunger. In contrast, neurons significantly responsive during satiety were rare and did not demonstrate a significant bias to the food cue or to hunger modulation (Extended Data Fig. 5).

Hunger modulation was consistently observed throughout granular (0.55 ± 0.03) and dysgranular (0.45 ± 0.03) subregions of InsCtx, without clear spatial organization (Fig. 2e). In contrast, early visual cortex responses were not substantially modulated by hunger using the identical experimental setup[16], arguing against global arousal driving InsCtx hunger modulation. To confirm this, we used moment-to-moment changes in pupil diameter as a proxy for changes in arousal[22] ($n = 266$ neurons, three additional mice; Fig. 2f, g). We selected pairs of single-trial InsCtx cue responses across hunger and satiety with similar arousal levels (matched pupil diameter in the 1 s before each cue; Fig. 2f and Extended Data Fig. 5e, f). This analysis removed low-arousal trials during satiety, resulting in a small increase in cue response magnitude (Fig. 2g) and in a 35% reduction in hunger modulation (0.54 ± 0.05 versus 0.35 ± 0.05). Importantly, however, food cue bias was unaffected, and significant hunger modulation persisted (Fig. 2g; $P = 4.3 \times 10^{-7}$, Wilcoxon signed-rank test, $n = 69$ neurons, three mice).

AgRP activation mimics hunger in InsCtx

AgRP neurons integrate peripheral signals of caloric deficit, and their activation is both necessary and sufficient for home-cage and instrumental feeding[14,15,23]. We hypothesized that AgRP neuron activation in sated mice could partly restore InsCtx food cue responses. Because AgRP neuron activity drops upon consumption of a large quantity of food[23–25], we first used fibre photometry[24] to determine whether activity remained roughly constant during our task, which involved food cues and consumption of a very small quantity of food (5 μl Ensure per trial). During hunger, visual food cues evoked a small, transient (10–15 s) drop in AgRP neuron activity, demonstrating that activity mostly remained high during the task (Extended Data Fig. 6 and Supplementary Discussion). These data validated a chemogenetic approach mimicking hunger in sated mice, via persistent activation of AgRP neurons (AAV8-DIO-hM3Dq–mCherry injection in the arcuate nucleus (ARC) of AgRP-ires-Cre mice and intraperitoneal injection of clozapine N-oxide (CNO)[15]), combined with InsCtx imaging (Fig. 3a).

First, we imaged InsCtx during the behavioural task across hunger (Hungry-1) and satiety (Sated-1). After satiation in the behavioural apparatus, mice occasionally resumed feeding within 30–60 min (Extended Data Fig. 7A, B). Thus, we allowed mice to fully satiate on chow in their home cage overnight. The following day, we imaged the same InsCtx neurons during satiety (Sated-2) and after activation of AgRP neurons (Sated-2 + AgRP). Remarkably, after AgRP activation, mice selectively licked to the food cue but withheld licking to other cues, similarly to Hungry-1 (Fig. 3b, c). Thus, AgRP activation mimics caloric deficiency-induced hunger not only in restoring instrumental
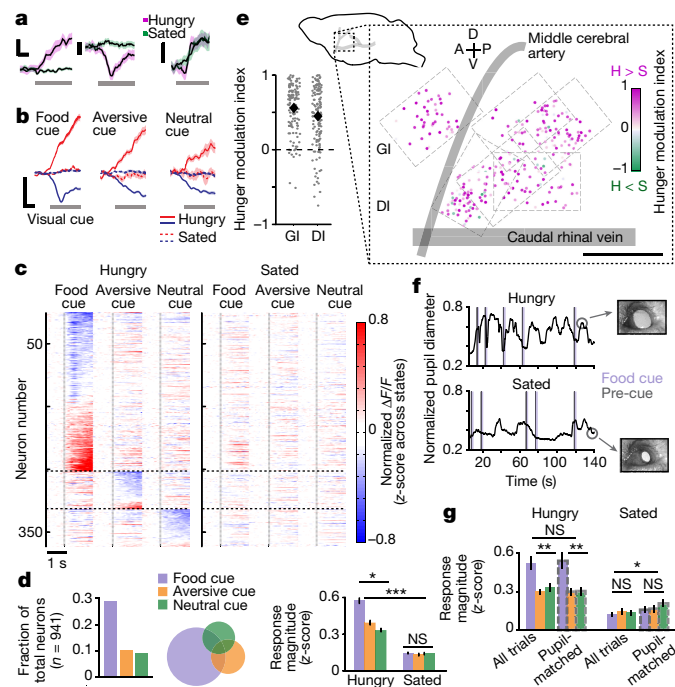
Figure 2 | Hunger gates InsCtx responses to learned visual cues.
a, Example single-neuron food cue responses during hunger and satiety. Scale bars, 0.5 s and normalized $\Delta F/F$ (fractional change in fluorescence, z-scored across states; left: 0.2; others: 0.1). **b**, Average population cue responses during hunger and satiety. Scale bars, 0.5 s and 0.3 normalized $\Delta F/F$. Mean ± s.e.m.; $n = 274$, 95, and 85 food, aversive, and neutral cue-responsive neurons, respectively; six mice. **c**, Average cue responses during hunger and satiety for cue-responsive neurons, grouped by the cue evoking the strongest response (horizontal dashed lines). Vertical dashed lines: visual cue onset. **d**, Fraction of cue-responsive neurons (left), response selectivity (middle), and magnitude (right); $n = 941$ neurons, six mice. Within-state: *$P = 2.8 \times 10^{-12}$ (Hungry); NS, $P = 0.6$ (Sated); Kruskal–Wallis test. Hungry: food versus aversive cue, $P = 1.7 \times 10^{-8}$; food versus neutral cue, $P = 7.3 \times 10^{-11}$; aversive versus neutral cue, $P = 0.01$. Hungry versus Sated: ***$P \leq 2.7 \times 10^{-19}$ for all cues, Mann–Whitney U-test. Mean ± s.e.m. **e**, Bottom left: hunger modulation index for all food-cue-responsive neurons (dots) in granular (GI) versus dysgranular (DI) subregions of InsCtx. Diamonds, means ($n = 274$ neurons, six mice). Top left: side view of mouse brain. Right: spatial map of hunger modulation index across cue-responsive neurons. H, hungry; S, sated. **f**, Pupil diameter dynamics during the discrimination task. **g**, Response magnitude, all trials versus pupil-matched trials. Within-state comparisons: **$P < 0.02$; NS, $P > 0.13$; Kruskal–Wallis test. Hungry: $P > 0.4$ for all cues; Sated: food cue, $P = 0.2$ ($n = 69$); aversive cue, $P = 0.6$ ($n = 39$); neutral cue, $P = 0.03$ ($n = 38$); Mann–Whitney U-test ($n = 3$ mice).

responding[15,23,25], but also in restoring selective operant responding to learned food cues.

We next asked how AgRP activation affects InsCtx cue responses ($n = 384$ neurons, four mice; Fig. 3d–f). The average cue response across all neurons in Hungry-1 was similarly attenuated during Sated-1 and Sated-2. Strikingly, AgRP activation during satiety restored InsCtx cue responsiveness to levels observed during hunger (Fig. 3d). AgRP activation, but not control saline injections, also restored InsCtx food cue bias and response magnitude across cue-responsive neurons (Figs 3e–f and Extended Data Fig. 7C, D). However, not all InsCtx neurons regained responsivity (Fig. 3g): while same-neuron responses were positively correlated only between Hungry-1 and Sated-2 + AgRP, the correlation coefficient was relatively low (0.35; Fig. 3h). Thus, we considered the state dependence of neurons that were food-cue-responsive during Hungry-1 (Fig. 3i). While only 23% responded similarly to the food cue in Hungry-1 versus Sated-2, this doubled to 47% in

Hungry-1 versus Sated-2 + AgRP (Fig. 3j). Surprisingly, this was comparable to response similarity across 2 hungry days ('Hungry versus Hungry-next-day'; Fig. 3j and Extended Data Fig. 7E), suggesting that AgRP activation during satiety restored the previous day's hunger pattern of cue-evoked responses as much as possible, given inherent day-to-day response variability of individual InsCtx neurons.

As InsCtx activity was necessary for task performance, we considered whether downstream neurons could use single-trial population activity patterns to extract cue information. We trained a simple decoder using single-trial population cue responses (90–98 neurons per mouse, $n = 4$ mice) in the Hungry-1 state, and asked whether it could predict which cue was presented using single-trial responses from other states. Prediction accuracy when testing on Hungry-next-day data was comparable to within-day accuracy (assessed across subsets of trials; Extended Data Fig. 7F). In contrast, accuracy dropped to chance when testing on Sated-1 or Sated-2 (Fig. 3k). Remarkably, when testing on next-day Sated-2 + AgRP, prediction accuracy was comparable to within-day accuracy (Fig. 3k). The response pattern was essential for decoding, as shuffling across neurons decreased accuracy to chance. Additionally, accurate decoding preceded licking (Extended Data Fig. 7G, H). These results suggest that single-trial InsCtx population activity is sufficient to discriminate among different learned visual cues to predict upcoming food availability, but only during hunger. AgRP activation during satiety was sufficient to restore InsCtx response patterns, such that food availability information could potentially be read out by downstream neurons. Consistent with results from other cortical regions[16,26], InsCtx preserves stable population response properties, despite variability in the average responses of individual neurons across days.

A pathway from AgRP neurons to InsCtx

InsCtx receives multiple ingestion-related visceral inputs, conveying diverse interoceptive information such as stomach stretch, visceral malaise, post-ingestive sugar absorption, and blood pressure[3,5,27]. These are conveyed to InsCtx via visceral thalamic, midbrain, and hindbrain nuclei[17]. Nevertheless, our findings suggest separate pathway(s) from AgRP neurons to InsCtx that could bypass and/or override visceral satiety pathways.

AgRP neurons do not project to InsCtx. Thus, we searched for pathways with one intermediate node (Fig. 4a). Retrogradely labelled InsCtx-projecting neurons (cholera toxin subunit B (CTB) conjugated to Alexa Fluor 488, injected in InsCtx) co-localized with AgRP axons at three sites: PVT, parasubthalamic nucleus, and lateral parabrachial nucleus (Fig. 4a). Using *ex vivo* channelrhodopsin-2-assisted circuit mapping[28] (CRACM), we found negligible AgRP inputs onto CTB-labelled neurons, in contrast to unlabelled neurons (Fig. 4a). This suggests that no single intermediate node connects AgRP neurons to InsCtx (Supplementary Discussion). Next, we conducted a broad survey of sites that are one or more synapses downstream of AgRP neurons, by injecting Cre-dependent trans-synaptic anterograde herpes simplex virus (HSV)[29] into the ARC of AgRP-ires-Cre mice. Three days later, labelled neurons (putatively one or two synapses downstream[29]) co-localized with AgRP axons in known targets regions. We also observed labelling in regions not innervated by AgRP axons, and the only such region projecting to InsCtx was BLA (Fig. 4b).

BLA encodes the value of learned cues[12,16,30,31], and is necessary for InsCtx responses to these cues[12]. BLA neurons that project to nucleus accumbens (NAc) and central amygdala (CeA) are important for behaviours involving cues predicting reward and punishment[32–34]. Interestingly, using rabies-based axon collateral mapping[35], we found that these and other BLA neurons all sent axon collaterals to InsCtx (Extended Data Fig. 8a).

We next searched for an intermediate node between AgRP neurons and BLA→InsCtx neurons, using projection-specific rabies monosynaptic tracing of inputs to BLA→InsCtx neurons. This labelled several
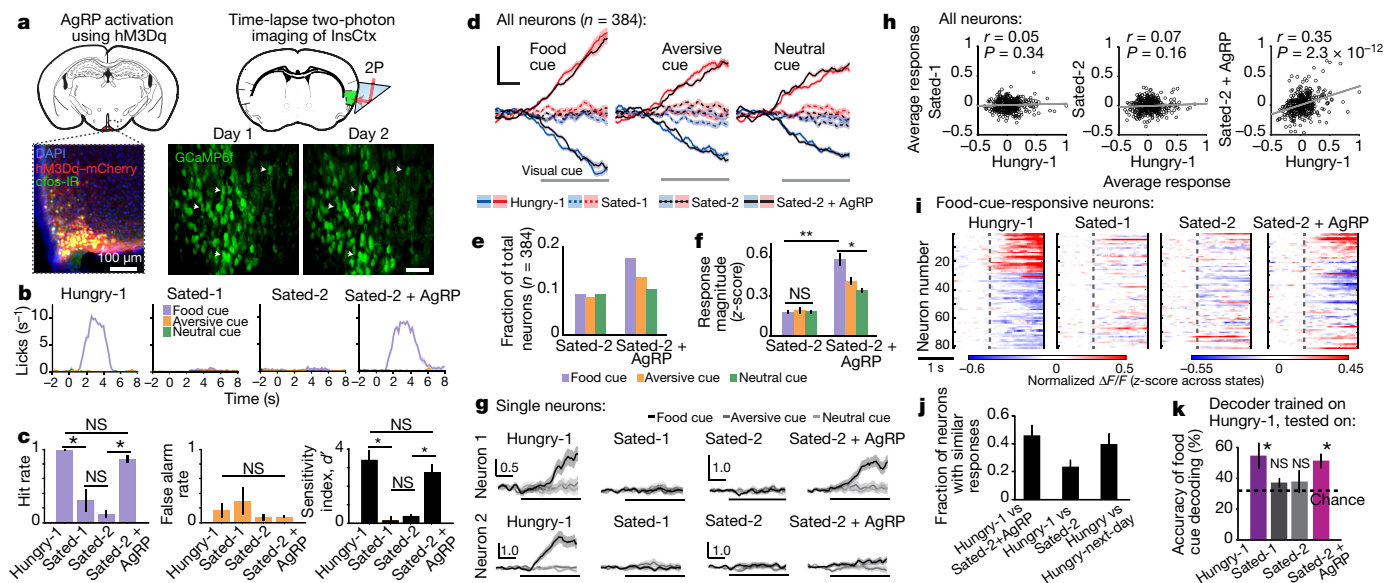
Figure 3 | Activation of AgRP neurons during satiety mimics hunger in InsCtx. a, AgRP activation while imaging InsCtx; 2P, two-photon. Brain schematics were adapted with permission from ref. 43. **b**, Example licking behaviour from one mouse. **c**, Behaviour across mice ($n = 4$). Hit rate across states, $P = 2.2 \times 10^{-5}$; Hungry-1 versus Sated-1, $P = 0.02$; Hungry-1 versus Sated-2, $P = 2.7 \times 10^{-4}$, Hungry-1 versus Sated-2 + AgRP, $P = 0.09$. False alarm rate across states, $P = 0.45$. Sensitivity index, d' (which combines hit rate and false alarm rate in a general measure of discrimination) across states, $P = 8.9 \times 10^{-5}$; Hungry-1 versus Sated-1, $P = 0.003$; Hungry-1 versus Sated-2, $P = 0.01$; Hungry-1 versus Sated-2 + AgRP, $P = 0.33$. Within-state and across-state comparisons: one-way ANOVA and Holm–Bonferroni-corrected paired t-tests, respectively. Mean ± s.e.m. **d**, Population cue responses of all neurons, averaged separately for cue-responsive neurons during Hungry-1 or Sated-2 + AgRP. Scale bars, 0.5 s, 0.1 normalized $\Delta F/F$, $n = 384$ neurons,

four mice. **e**, Proportions of cue-responsive neurons; $n = 384$ neurons, four mice. **f**, Response magnitude. Within-state, $*P = 2.6 \times 10^{-4}$ (Sated-2 + AgRP); NS, $P = 0.8$ (Sated-2); Kruskal–Wallis test. Sated-2 + AgRP: food versus aversive cue, $P = 0.005$; food versus neutral cue, $P = 5.8 \times 10^{-5}$; aversive versus neutral cue, $P = 0.03$. Sated-2 + AgRP versus Sated-2, $**P \leq 1.2 \times 10^{-8}$ for all cues. Mann–Whitney U-test. Mean ± s.e.m. **g**, Example neurons. Scale bars, 0.5 s and normalized $\Delta F/F$. **h**, Average food cue responses from all neurons across states ($n = 384$ neurons, four mice). Mean ± s.e.m. **i**, Time courses for food-cue-responsive neurons. **j**, Fraction of food-cue-responsive neurons that responded similarly across states ($n = 81$ neurons, four mice), and across 'Hungry versus Hungry-next-day' ($n = 59$ neurons, four mice). Mean ± s.e.m. across mice. **k**, Food cue decoding accuracy. Mean ± s.e.m. $*P \leq 0.03$, t-test versus chance accuracy (33.3%), $n = 4$ mice (90–98 neurons per mouse).

sites (Extended Data Fig. 8b–d), but the major site that co-localized with AgRP axons was PVT (Fig. 4c). PVT is involved in motivated behaviours[36] including feeding[37,38], and AgRP$^{\rightarrow PVT}$ stimulation induces feeding[35]. Using CRACM, we found that BLA$^{\rightarrow InsCtx}$ neurons and BLA inhibitory interneurons received synaptic input from PVT (Extended Data Fig. 8e). Neurons were also labelled in bed nucleus of the stria terminalis (BNST; ruled out using CRACM) and ventrolateral peri-aqueductal grey (unlikely to be directly involved; Supplementary Discussion and Extended Data Fig. 8f).

These results implicate a pathway from AgRP neurons to BLA$^{\rightarrow InsCtx}$ neurons via PVT. Using CRACM, we found that most PVT$^{\rightarrow BLA}$ neurons received AgRP input (15 out of 22; Fig. 4d). Using rabies-based collateral mapping[35], we found PVT$^{\rightarrow BLA}$ axon collaterals in NAc/BNST[39], but not in other PVT targets, including CeA[40,41]. In contrast, PVT$^{\rightarrow NAc/BNST}$ neurons collateralized in all examined PVT targets (Extended Data Fig. 9A–C). Thus, while NAc/BNST is a major projection target of PVT[36], distinct PVT subsets project to BLA or CeA and probably serve different behavioural functions[41].

We next tested whether AgRP neurons preferentially target PVT$^{\rightarrow BLA}$ neurons within the PVT, using CRACM of AgRP inputs onto different PVT populations (Fig. 4e). Remarkably, most PVT$^{\rightarrow BLA}$ neurons received input from AgRP neurons (~70%; 15 out of 22), while lower connectivity rates were observed for other PVT subsets (for example, ~5% of PVT$^{\rightarrow InsCtx}$; Fig. 4e and Supplementary Discussion) and for randomly sampled PVT neurons (~20%; 5 out of 26).

To test the contribution of this pathway to behaviour and InsCtx activity, we performed several pathway-specific manipulations. First, as AgRP neurons are inhibitory, inhibition of PVT$^{\rightarrow BLA}$ neurons in fed mice should increase feeding[35]. We achieved selective chemogenetic

inhibition of PVT$^{\rightarrow BLA}$ neurons by injecting retrogradely trafficking AAV6-Cre–GFP in BLA and AAV8-DIO-hM4Di–mCherry in PVT. Inhibition of PVT$^{\rightarrow BLA}$ neurons significantly increased home-cage feeding (Fig. 4f). Interestingly, this effect was smaller than that evoked by activating AgRP$^{\rightarrow PVT}$ axons[35], potentially owing to technical factors (partial penetrance/efficacy). However, because AgRP neurons also target other PVT neurons (Fig. 4e), we hypothesized that PVT$^{\rightarrow BLA}$ neurons specifically control responses to predictive cues, thereby explaining this partial effect.

To test this in the discrimination task, we performed chemogenetic stimulation of PVT$^{\rightarrow BLA}$ neurons (Fig. 4g). During hunger, this should occlude persistent AgRP-mediated inhibition[25] (Extended Data Fig. 6) of PVT$^{\rightarrow BLA}$ neurons, thereby reducing behavioural performance. We used a 2-day protocol with two blocks after saline injections on day 1 (Saline-1.1, Saline-1.2). On day 2, the second block followed CNO injection (Saline-2.1, CNO-2.2). Stimulation of PVT$^{\rightarrow BLA}$ neurons selectively reduced behavioural responses to the food cue, and did not affect licking behaviour (Fig. 4g and Extended Data Fig. 9D).

Pharmacological BLA silencing attenuates InsCtx learned cue responses in thirsty rats[12]. However, this could be mediated by indirect and/or direct pathways. To specifically test the contribution of BLA$^{\rightarrow InsCtx}$ neurons to InsCtx cue responses, we combined selective chemogenetic inhibition of BLA$^{\rightarrow InsCtx}$ neurons (injecting AAV6-Cre in InsCtx and AAV8-DIO-hM4Di–mCherry in BLA) with InsCtx imaging. We imaged the same neurons during the 2-day protocol described above (Fig. 5a; $n = 350$ neurons, four mice). In some neurons, food cue responses were stable across saline sessions, but decreased after BLA$^{\rightarrow InsCtx}$ inhibition. In others, responses were unaffected (Fig. 5b).
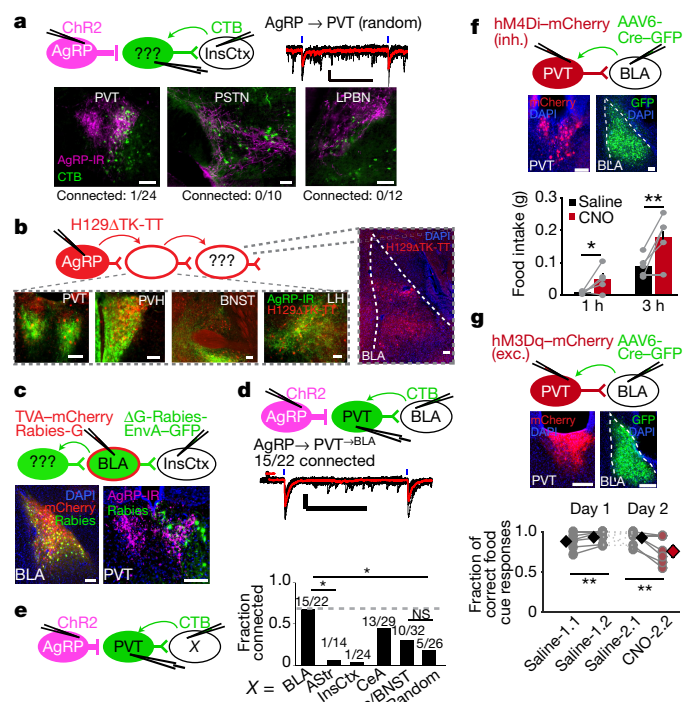
Figure 4 | A neural pathway from hypothalamic AgRP neurons to InsCtx. a, Top: AgRP connectivity with InsCtx-projecting neurons. Black lines: 15 sweeps; red line: average; blue lines: light stimulation. Scale bars, 30 pA, 500 ms. Bottom: CTB-labelled neurons co-localized with AgRP axons, and CRACM connectivity. Scale bars, 100 μm. **b**, Top: Cre-dependent anterograde HSV tracing. Bottom: images from known AgRP target areas, demonstrating HSV-labelled somata co-localized with AgRP axons. Right: HSV-labelling in BLA. Scale bars, 100 μm. PVH: paraventricular hypothalamus, LH: lateral hypothalamus. **c**, Rabies-based, projection-specific monosynaptic tracing of inputs to BLA$^{→InsCtx}$ neurons. Scale bars, 100 μm. **d**, CRACM from AgRP neurons onto PVT$^{→BLA}$ neurons. Scale bars, 50 pA, 500 ms. **e**, Left: CRACM from AgRP neurons onto PVT neurons projecting to different targets ('X'). Right: connectivity summary. *$P ≤ 0.04$ (binomial proportions test, Holm–Bonferroni corrected). **f**, Top: PVT$^{→BLA}$ inhibition (inh.), and images of BLA and PVT. Scale bars, 100 μm. Bottom: home-cage feeding; dots, individual mice. *$P = 0.03$, **$P = 0.01$, paired t-test ($n = 5$ mice). **g**, Same as **f**, but for (top) PVT$^{→BLA}$ excitation (exc.). Scale bars, 200 μm. Bottom: discrimination task performance; dots, individual mice; diamonds and error bars, mean ± s.e.m.; NS, $P ≥ 0.2$; **$P < 0.02$, paired t-test ($n = 6$ mice).

Across the population, responses were stable on day 1 (Saline-1.1 versus Saline-1.2), but were attenuated on day 2 after BLA$^{→InsCtx}$ inhibition (Saline-2.1 versus CNO-2.1; Fig. 5c, d), regardless of whether inhibition was bilateral ($n = 2$) or ipsilateral ($n = 2$). However, only bilateral inhibition reduced incidence (but not latency or vigour) of behavioural licking responses to food cues. InsCtx food cue responses were significantly attenuated, even when restricting analysis to trials with correct behavioural responses (Extended Data Fig. 10). In contrast, InsCtx responses to Ensure consumption were unaffected by BLA$^{→InsCtx}$ inhibition (Fig. 5e, f), consistent with pharmacological BLA silencing in thirsty rats[12,42]. BLA$^{→InsCtx}$ inhibition attenuated responses to all three cues. However, the strongest attenuation was of food cue responses, thereby reducing food cue bias in InsCtx (Fig. 5g).

Discussion

We propose the following model (Fig. 5h and Supplementary Discussion). Caloric deficiency increases AgRP neuron activity[25], thereby inhibiting PVT, especially PVT$^{→BLA}$ neurons (Fig. 4e). BLA represents the valence of learned cues[30,31], and may receive visual information from lateral-posterior thalamus and postrhinal cortex[16] (mouse homologues of pulvinar and parahippocampal cortex; Extended Data
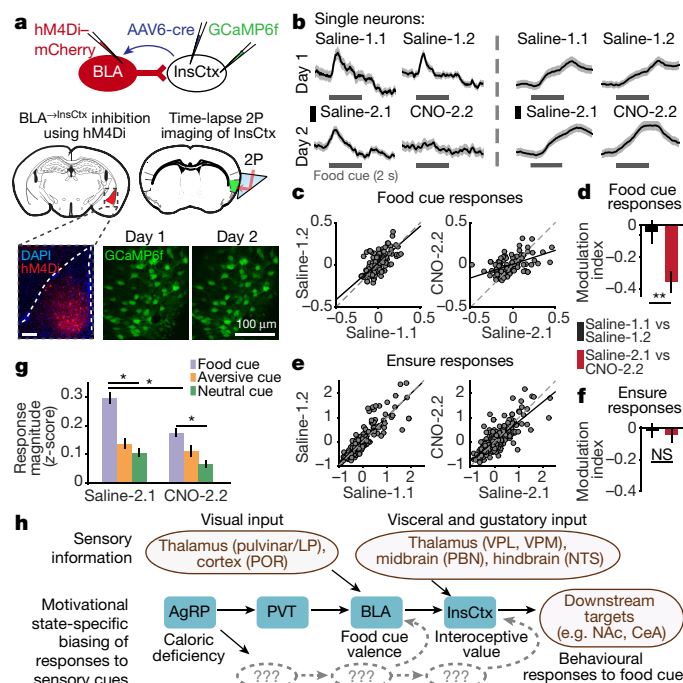

Figure 5 | Inhibition of BLA$^{→InsCtx}$ neurons attenuates food cue responses in InsCtx. a, Inhibition of BLA$^{→InsCtx}$ neurons while imaging InsCtx. Brain schematics were adapted with permission from ref. 43. **b**, Example single neurons. Scale bars, 0.2 normalized $\Delta F/F$. **c**, Average cue-evoked responses for food-cue-responsive neurons. Dots, individual neurons. Linear regression line, black; line of unity, dashed grey. **d**, Modulation index. Median ± s.e. median. **$P = 0.001$, Mann–Whitney U-test, $n = 98$ neurons, four mice. **e**, Average Ensure-evoked responses. **f**, Modulation index. Median ± s.e. median. NS, $P = 0.5$; Mann–Whitney U-test, $n = 176$ neurons, four mice. **g**, Cue response magnitude. Within condition, *$P < 3.9 × 10^{-7}$, Kruskal–Wallis test. Saline-2.1: food versus aversive, $P = 6.2 × 10^{-9}$; food versus neutral, $P = 4.2 × 10^{-9}$; aversive versus neutral, $P = 0.6$; CNO-2.2: food versus aversive, $P = 1.5 × 10^{-4}$; food versus neutral, $P = 5 × 10^{-9}$; aversive versus neutral, $P = 0.2$; Saline-2.1 versus CNO-2.2: food, $P = 1.7 × 10^{-8}$; aversive, $P = 0.04$; neutral, $P = 0.01$, Mann–Whitney U-test ($n = 118$, 57, and 36 food, aversive, and neutral cue-responsive neurons, respectively, four mice). **h**, Pathway from AgRP neurons to InsCtx. Grey, additional unknown pathways (Supplementary Discussion). LP, lateral-posterior thalamus; POR, postrhinal cortex; VPL, ventroposterior lateral thalamus; VPM, ventroposterior medial thalamus; PBN, parabrachial nucleus; NTS, nucleus of the solitary tract.

Fig. 8c). Hunger-dependent enhancement of food cue responses may already occur in BLA[12,16] (Figs 4 and 5). Therefore, during satiety, PVT may attenuate the food cue responses of BLA$^{→InsCtx}$ neurons, possibly by preferential excitation of BLA inhibitory interneurons (Extended Data Fig. 8e). In contrast, during hunger, AgRP inhibition of PVT$^{→BLA}$ neurons would disinhibit BLA$^{→InsCtx}$ neurons, allowing them to relay cue information to InsCtx[12] (Fig. 5). InsCtx could then integrate cue information from BLA with other visceral and gustatory inputs from hindbrain, midbrain, and thalamus, to form an integrated representation of these cues and their predicted interoceptive outcomes (for example, stomach stretch and nutrient absorption).

We used a behavioural task involving both appetitive and aversive cues, and found that it required InsCtx, while feeding per se did not. We therefore suggest that InsCtx influences action selection by weighing the predicted interoceptive consequences associated with responding to learned cues in the context of current physiological needs[2]. Thus, state-specific gating of InsCtx, and the pathway we uncovered, provide a framework for future studies exploring how natural and pathological need states bias the weighing of positive and negative interoceptive consequences in InsCtx.

1. Frank, S., Kullmann, S. & Veit, R. Food related processes in the insular cortex. *Front. Hum. Neurosci.* **7,** 499 (2013).
2. Naqvi, N. H., Gaznick, N., Tranel, D. & Bechara, A. The insula: a critical neural substrate for craving and drug seeking under conflict and risk. *Ann. NY Acad. Sci.* **1316,** 53–70 (2014).
3. Cechetto, D. F. & Saper, C. B. Evidence for a viscerotopic sensory representation in the cortex and thalamus in the rat. *J. Comp. Neurol.* **262,** 27–45 (1987).
4. de Araujo, I. E. *et al.* Neural ensemble coding of satiety states. *Neuron* **51,** 483–494 (2006).
5. Hanamori, T., Kunitake, T., Kato, K. & Kannan, H. Responses of neurons in the insular cortex to gustatory, visceral, and nociceptive stimuli in rats. *J. Neurophysiol.* **79,** 2535–2545 (1998).
6. Huerta, C. I., Sarkar, P. R., Duong, T. Q., Laird, A. R. & Fox, P. T. Neural bases of food perception: coordinate-based meta-analyses of neuroimaging studies in multiple modalities. *Obesity (Silver Spring)* **22,** 1439–1446 (2014).
7. Cornier, M. A. *et al.* The effects of overfeeding on the neuronal response to visual food cues in thin and reduced-obese individuals. *PLoS ONE* **4,** e6310 (2009).
8. Schienle, A., Schäfer, A., Hermann, A. & Vaitl, D. Binge-eating disorder: reward sensitivity and brain activation to images of food. *Biol. Psychiatry* **65,** 654–661 (2009).
9. Gardner, M. P. & Fontanini, A. Encoding and tracking of outcome-specific expectancy in the gustatory cortex of alert rats. *J. Neurosci.* **34,** 13000–13017 (2014).
10. Kusumoto-Yoshida, I., Liu, H., Chen, B. T., Fontanini, A. & Bonci, A. Central role for the insular cortex in mediating conditioned responses to anticipatory cues. *Proc. Natl Acad. Sci. USA* **112,** 1190–1195 (2015).
11. Saddoris, M. P., Holland, P. C. & Gallagher, M. Associatively learned representations of taste outcomes activate taste-encoding neural ensembles in gustatory cortex. *J. Neurosci.* **29,** 15386–15396 (2009).
12. Samuelsen, C. L., Gardner, M. P. & Fontanini, A. Effects of cue-triggered expectation on cortical processing of taste. *Neuron* **74,** 410–422 (2012).
13. Parkes, S. L. & Balleine, B. W. Incentive memory: evidence the basolateral amygdala encodes and the insular cortex retrieves outcome values to guide choice between goal-directed actions. *J. Neurosci.* **33,** 8753–8763 (2013).
14. Aponte, Y., Atasoy, D. & Sternson, S. M. AGRP neurons are sufficient to orchestrate feeding behavior rapidly and without training. *Nat. Neurosci.* **14,** 351–355 (2011).
15. Krashes, M. J. *et al.* Rapid, reversible activation of AgRP neurons drives feeding behavior in mice. *J. Clin. Invest.* **121,** 1424–1428 (2011).
16. Burgess, C. R. *et al.* Hunger-dependent enhancement of food cue responses in mouse postrhinal cortex and lateral amygdala. *Neuron* **91,** 1154–1169 (2016).
17. Saper, C. B. The central autonomic nervous system: conscious visceral perception and autonomic pattern generation. *Annu. Rev. Neurosci.* **25,** 433–469 (2002).
18. Accolla, R. & Carleton, A. Internal body state influences topographical plasticity of sensory representations in the rat gustatory cortex. *Proc. Natl Acad. Sci. USA* **105,** 4010–4015 (2008).
19. Chen, X., Gabitto, M., Peng, Y., Ryba, N. J. & Zuker, C. S. A gustotopic map of taste qualities in the mammalian brain. *Science* **333,** 1262–1266 (2011).
20. Andermann, M. L. *et al.* Chronic cellular imaging of entire cortical columns in awake mice using microprisms. *Neuron* **80,** 900–913 (2013).
21. Katz, D. B., Simon, S. A. & Nicolelis, M. A. Dynamic and multimodal responses of gustatory cortical neurons in awake rats. *J. Neurosci.* **21,** 4478–4489 (2001).
22. Reimer, J. *et al.* Pupil fluctuations track rapid changes in adrenergic and cholinergic activity in cortex. *Nat. Commun.* **7,** 13289 (2016).
23. Betley, J. N. *et al.* Neurons for hunger and thirst transmit a negative-valence teaching signal. *Nature* **521,** 180–185 (2015).
24. Chen, Y., Lin, Y. C., Kuo, T. W. & Knight, Z. A. Sensory detection of food rapidly modulates arcuate feeding circuits. *Cell* **160,** 829–841 (2015).
25. Mandelblat-Cerf, Y. *et al.* Arcuate hypothalamic AgRP and putative POMC neurons show opposite changes in spiking across multiple timescales. *eLife* **4,** e07122 (2015).
26. Huber, D. *et al.* Multiple dynamic representations in the motor cortex during sensorimotor learning. *Nature* **484,** 473–478 (2012).
27. Oliveira-Maia, A. J. *et al.* The insular cortex controls food preferences independently of taste receptor signaling. *Front. Syst. Neurosci.* **6,** 5 (2012).
28. Petreanu, L., Huber, D., Sobczyk, A. & Svoboda, K. Channelrhodopsin-2-assisted circuit mapping of long-range callosal projections. *Nat. Neurosci.* **10,** 663–668 (2007).
29. Lo, L. & Anderson, D. J. A Cre-dependent, anterograde transsynaptic viral tracer for mapping output pathways of genetically marked neurons. *Neuron* **72,** 938–950 (2011).
30. Baxter, M. G. & Murray, E. A. The amygdala and reward. *Nat. Rev. Neurosci.* **3,** 563–573 (2002).
31. Morrison, S. E. & Salzman, C. D. Re-valuing the amygdala. *Curr. Opin. Neurobiol.* **20,** 221–230 (2010).
32. Kim, J., Pignatelli, M., Xu, S., Itohara, S. & Tonegawa, S. Antagonistic negative and positive neurons of the basolateral amygdala. *Nat. Neurosci.* **19,** 1636–1646 (2016).
33. Namburi, P. *et al.* A circuit mechanism for differentiating positive and negative associations. *Nature* **520,** 675–678 (2015).
34. Stuber, G. D. *et al.* Excitatory transmission from the amygdala to nucleus accumbens facilitates reward seeking. *Nature* **475,** 377–380 (2011).
35. Betley, J. N., Cao, Z. F., Ritola, K. D. & Sternson, S. M. Parallel, redundant circuit organization for homeostatic control of feeding behavior. *Cell* **155,** 1337–1350 (2013).
36. Kirouac, G. J. Placing the paraventricular nucleus of the thalamus within the brain circuits that control behavior. *Neurosci. Biobehav. Rev.* **56,** 315–329 (2015).
37. Labouèbe, G., Boutrel, B., Tarussio, D. & Thorens, B. Glucose-responsive neurons of the paraventricular thalamus control sucrose-seeking behavior. *Nat. Neurosci.* **19,** 999–1002 (2016).
38. Stratford, T. R. & Wirtshafter, D. Injections of muscimol into the paraventricular thalamic nucleus, but not mediodorsal thalamic nuclei, induce feeding in rats. *Brain Res.* **1490,** 128–133 (2013).
39. Zhu, Y., Wienecke, C. F., Nachtrab, G. & Chen, X. A thalamic input to the nucleus accumbens mediates opiate dependence. *Nature* **530,** 219–222 (2016).
40. Do-Monte, F. H., Quiñones-Laracuente, K. & Quirk, G. J. A temporal shift in the circuits mediating retrieval of fear memory. *Nature* **519,** 460–463 (2015).
41. Penzo, M. A. *et al.* The paraventricular thalamus controls a central amygdala fear circuit. *Nature* **519,** 455–459 (2015).
42. Piette, C. E., Baez-Santiago, M. A., Reid, E. E., Katz, D. B. & Moran, A. Inactivation of basolateral amygdala specifically eliminates palatability-related information in cortical sensory responses. *J. Neurosci.* **32,** 9981–9991 (2012).
43. Paxinos, G. & Franklin, K. B. J. *The Mouse Brain in Stereotaxic Coordinates* (Elsevier Academic Press, 2004).

Author Contributions Y.L., B.B.L., and M.L.A. designed the experiments and wrote the manuscript. Y.L. performed all imaging, feeding studies, pharmacological silencing, and data analyses. Y.L. and K.M.L. performed circuit mapping. Y.L., G.J.G., and M.L.A. developed the InsCtx microprism surgery. Y.L. and V.E.D. performed fibre photometry. J.C.M. and H.F. performed slice electrophysiology. Y.L. and N.J. performed locomotion experiments. R.N.R. assisted with data analysis and provided conceptual input. C.R.B. assisted with initial imaging and AgRP activation, and provided conceptual input. J.M.R. assisted with initial pharmacological silencing.

METHODS

All animal care and experimental procedures were approved by the Beth Israel Deaconess Medical Center Institutional Animal Care and Use Committee. Animals were housed with standard mouse chow and water provided *ad libitum*, unless specified otherwise. We used male mice only. Sample sizes were chosen to reliably measure experimental parameters while keeping with standards in the relevant fields[19,28,44,45], and remaining in compliance with ethical guidelines to minimize the number of animals used. Experiments did not involve experimenter-blinding, but randomization was used with respect to trial order and data collection. Animal subjects were not randomly allocated to experimental groups as all comparisons were performed within subject.

Behavioural training. See Supplementary Methods for a more detailed description. Behavioural training was performed as previously described[16]. Briefly, we food-restricted animals (to 85% of free-feeding body weight) and habituated them to head fixation. We trained animals to lick for drops of Ensure (5 μl, 0.0075 kcal, each). We then introduced the 'go' visual food cue, initially paired with unconditional (Pavlovian) delivery of Ensure. Once animals exhibited anticipatory licking, we transitioned them to operant delivery of Ensure, conditional on licking during the 2 s after food cue offset. After animals reliably licked to the operant food cue (in >80% of trials), we introduced 'no-go' trials involving presentation of an operant quinine-predicting cue (delivery of 5 μl of 1 mM quinine) and of a neutral cue (no outcome). Initially, we biased the total number of trials towards the food cue, and then gradually increased the fraction of other cue trials so that all visual cues were eventually presented in equal proportions. Animals typically learned to perform this task in ~2 weeks. Visual cues (presented for 2 s, every 8–10 s) were square-wave drifting gratings differing in orientation. Mice were considered well-trained on the basis of the following criteria: licking to >80% of food cue trials (usually about 90–95%) and licking to <50% of other cue trials (usually about 10–20%).

Switching cue–outcome associations in well-trained mice. We first trained mice with the same cue–outcome associations and training protocol described above, and imaged InsCtx once mice were well-trained. Then, we switched cue–outcome associations such that the visual grating associated with the neutral outcome became associated with the food outcome, and vice versa (the aversive cue remained unchanged). To address the potential effects of biased overexposure to one visual stimulus during early training, we kept the number of presentations of the three stimuli strictly equal throughout re-training on the new cue–outcome associations. Once mice were deemed successfully re-trained (on the basis of the criteria above), we re-imaged the same InsCtx fields of view in these mice.

Surgical procedures. See Supplementary Methods for a more detailed description of all surgical procedures described below.

Cannula implantation. Cannula implantation was performed using AgRP-ires-Cre mice (10–16 weeks old) as described previously[10], and a custom-made headpost was glued to the skull.

Stereotactic injections. Stereotaxic injections were performed as previously described[44]. Mice were 8–14 weeks old at the time of injection, except for CRACM experiments, for which mice were 5–10 weeks old.

We used the following volumes of virus and injection coordinates: InsCtx (100–200 nl, Bregma: anteroposterior (AP) 0.0/0.8 mm, dorsoventral (DV) −4.1/−4.3 mm, mediolateral (ML) ~4.0 mm); ARC (200 nl, Bregma: AP −1.45 mm, DV −5.85 mm, ML ±0.25 mm); PVT (25–50 nl, Bregma: AP −1.0/−1.3 mm, DV −3.0/−3.0 mm, ML 0.0/0.0 mm); BLA (100 nl, Bregma: AP −1.6 mm, DV −4.5/−4.76 mm, ML ±3.3 mm); CeA (50 nl, Bregma: AP −0.75 mm, DV −5.1 mm, ML ±2.3 mm); NAc (100 nl, Bregma: AP 1.4 mm, DV −4.7 mm, ML ±0.85 mm).

We used the following viruses: AAV1-hSyn-GCaMP6f (UPenn), AAV1-hSyn-GCaMP6s (UNC), AAV8-DIO-hM3Dq–mCherry (UNC), AAV8-DIO-hM4Di–mCherry (UNC), AAV8-DIO-ChR2(H134R)–mCherry (UNC), AAV5-hSyn-ChR2(H134R)-EYFP (UNC), AAV8-FLEX-TVA–mCherry, (UNC), AAV8-FLEX-RG–mCherry, (UNC), SADΔG–EGFP (EnvA) rabies (Salk), AAV6-CAG-cre–GFP; (Boston Children's Hospital), H129ΔTK-TT (Center for Neuroanatomy with Neurotropic Viruses, strain H356).

Optic fibre implantation for fibre photometry. Mice were first stereotactically injected with AAV1-hSyn-GCaMP6s into the ARC. An optic fibre (400 μm diameter core; numerical aperture 0.37; Thorlabs) with a metal ferrule was then implanted unilaterally over the ARC (AP −1.45 mm, DV −5.8 mm, ML 0.3 mm from Bregma). The fibre and a custom-made headpost were then glued to the skull.

Microprism assembly and surgery. Glass microprism assemblies were fabricated using standard 2 mm prisms (MCPH-1.0; Tower Optical) coated with aluminium along their hypotenuse[20]. Prisms were attached to a coverglass (#1 thickness), both along the hypotenuse (to prevent scratching of the reflective surface) and at the side of the prism facing InsCtx, using Norland Optical Adhesive.

Approximately 1–2 weeks after AAV-GCaMP6f[46] injection into InsCtx, AgRP-ires-Cre or C57BL/6 mice (10–16 weeks old) were anaesthetized using isoflurane in 100% O₂ (induction, 3%; maintenance, 1–1.5%). Using aseptic technique, a custom-made headpost was secured using C&B Metabond (Parkell). A 2.2 mm × 2.2 mm craniotomy was then performed over the left InsCtx (bottom edge of the craniotomy was just above the squamosal plate), centred around the AAV-GCaMP6f injection site. The microprism was then stereotactically lowered into the craniotomy, while verifying that the microprism's bottom edge was inserted below the squamosal plate. Once the prism was in place, the window edges were affixed to the skull using Vetbond (3M), followed by C&B Metabond (Parkell). Meloxicam (0.5 mg per kg (body weight), subcutaneously) and a prophylactic antibiotic (cefazolin; 500 mg per kg (body weight), subcutaneously) were administered.

Pharmacological silencing. See Supplementary Methods for a more detailed description. Pharmacological silencing was performed as previously described[10], except that 1 min after infusion, injection cannulae were replaced with dummy cannulae, and behavioural testing began 15 min later. We verified cannula location for every animal and included all animals with cannulae in InsCtx in subsequent analyses.

For testing performance on the visual discrimination task, food-restricted mice (~85% of free-feeding weight) performed two runs per day. The first run was always a saline infusion run and the second run was either a drug infusion run or another saline run (controlling for time elapsed and Ensure consumed).

For testing locomotion in the home cage, food-restricted mice were head-fixed and infused with saline/drug (on separate days), and then returned to their home cage. Fifteen minutes after infusion, a 30 min video recording began using a camera (Point Grey, Flea3 FL3-U3-13Y3M) above the home cage. For each frame, mice were segmented to obtain coordinates of centre-of-mass, used to compute position and locomotion.

For testing feeding on chow in the home cage, food-restricted mice were head-fixed and infused with saline/drug (on separate days), and then returned to their home cage. Fifteen minutes after infusion, a large food pellet (regular chow, ~4 g) was inserted into the home cage. The food pellet was weighed every 30 min.

For testing feeding on Ensure while head-fixed on the trackball, food-restricted mice were head-fixed and infused with saline/drug (on separate days). Uniform grey illumination was presented instead of visual stimuli. Fifteen minutes after infusion, we began a 30 min run in which licking triggered delivery of Ensure (5 μl; 2.5 s minimum interval between Ensure deliveries). Mice usually consumed 2–3 ml of Ensure during this period.

Two-photon imaging across hunger, satiety, activation of AgRP neurons, inhibition of BLA→InsCtx neurons, and in naive mice. See Supplementary Methods for a more detailed description. Two-photon imaging was performed using a resonant-scanning two-photon microscope with tiltable scanhead (Neurolabware; 31 frames per second; 1,154 pixels × 512 pixels). All imaging was performed with a 20×, 0.45 numerical aperture air objective (Olympus) with a 540 μm × 360 μm field of view. All fields of view were imaged at a depth of 90–150 μm, using a Mai Tai DeepSee laser (Newport) with laser power at 920–960 nm of 35–80 mW at the front aperture of the objective (power at the sample was probably substantially less because of partial transmission via the microprism).

To assay how changes in hunger state affected behavioural and neural activity, we imaged in two blocks of ~180 trials within a session (trial duration 8–10 s), one during hunger (food-restriction) and a subsequent block immediately after re-feeding (satiety; after *ad libitum* access to Ensure for 45–75 min, consumption of ~3–5 ml, eventually causing voluntarily cessation of licking[16]). Using this satiation protocol, we found that mice could occasionally resume feeding within 30–60 min. In such cases, the imaging run was aborted, and mice were allowed to consume more Ensure *ad libitum* before restarting the imaging run. 'Sated' runs did not have licking in >70% of trials. This re-satiation was necessary only in a subset of mice and only in ~30% of post-satiation sessions (see examples in Extended Data Fig. 7A, B).

For experiments involving chemogenetic activation of AgRP neurons, after imaging during hunger and satiety, mice were returned to their home cage with *ad libitum* access to regular chow. The next morning, we imaged the same InsCtx field of view in this satiety state (100–110% of normal body weight) during ~180 trials (30 min). We then injected CNO (1–3 mg per kg (body weight), intraperitoneally). Ten minutes later, we initiated an additional imaging run of ~180 trials. The effects of CNO injections were not due to the actual pain caused by the injection, as saline injections did not restore behavioural responses or neuronal responses (Extended Data Fig. 7D). For every mouse used for these experiments, post-mortem histology and immunohistochemistry (see below) confirmed hM3Dq–mCherry expression in the ARC.

For experiments involving chemogenetic inhibition of BLA→InsCtx neurons, we first performed bilateral injections of AAV6-Cre[47] into InsCtx and

AAV8-DIO-hM4Di–mCherry into BLA of C57BL/6 mice. We injected AAV1-hSyn-GCaMP6f into InsCtx 1–2 weeks later. We then performed InsCtx microprism surgeries 1–2 weeks later. After an additional 4–6 weeks, we ran a 2-day protocol, two blocks per day, each after injection of either saline or CNO (10 mg per kg (body weight)). We started imaging 10 min after injection. We only analysed mice with hits either bilateral or ipsilateral to the InsCtx microprism, assessed using post-mortem histology.

For experiments involving naive mice (before learning the behavioural task), mice were habituated to head-restraint, and food-restricted (~85% normal body weight). Mice were then head-fixed under the two-photon microscope in the absence of a lick-spout, and underwent one 30-min habituation session with presentation of the visual cue sequence described above. InsCtx was then imaged during a second identical 30 min session.

Pupil and orofacial videography during two-photon imaging. We acquired data using a GigE Vision video-rate camera (Dalsa; 15 Hz) with a 60-mm lens (Nikon) from a pre-selected region of interest around the eye ipsilateral to visual cue presentation (contralateral to the InsCtx microprism), or around the orofacial region. The pupil was illuminated by spread of two-photon excitation infrared light from within the brain.

Post-mortem identification of imaging field location. Mice were terminally anaesthetized with an overdose of chloral hydrate (Sigma Aldrich), decapitated after several hours to reduce blood loss, and heads were post-fixed in 10% formalin (Fisher Scientific). We used light and fluorescence microscopy for visualization of surface vasculature and GCaMP6f fluorescence. Microprism location was evident by a minor indentation of the tissue. We aligned the post-mortem surface vasculature to *in vivo* microprism epifluorescence images and then to vascular landmarks from *in vivo* two-photon imaging. We used this to localize imaging fields, relative to the middle cerebral artery and rhinal vein. We broadly classified imaging fields either in granular or dysgranular subregions of InsCtx on the basis of proximity to the rhinal vein and of subsequent examination of coronal sections.

Brain tissue preparation and immunohistochemistry. Histology was performed as previously described[44]. We used the following primary antibodies: rabbit anti-dsRed, Clonetech (632496) 1:1,000; chicken anti-GFP, Life Technologies (A10262) 1:1,000; goat anti-AgRP, Neuromics (GT15023) 1:1,000; rabbit anti-cfos, Santa-Cruz (sc-52) 1:1,000.

Anterograde HSV, rabies collateral mapping, projection-specific monosynaptic rabies tracing, and CRACM. Experiments were all performed similarly to previously described procedures[44,48,49], but with slight modifications. See Supplementary Methods for a more detailed description.

Food intake studies after chemogenetic inhibition of PVT→BLA neurons. See Supplementary Methods for a more detailed description. Briefly, we assessed food intake after mice received injections of saline on day 1 and CNO (10 mg per kg (body weight)) on day 2. A complete experiment involved repetition of these measurements once a week for 3 weeks. Data for each mouse were an average of the three repetitions of each condition.

Behavioural studies during the visual discrimination task after chemogenetic excitation of PVT→BLA neurons. See Supplementary Methods for a more detailed description. Briefly, the procedure was similar to the pharmacological silencing described above, but using intraperitoneal injections of saline or CNO (10 mg per kg (body weight)).

Fibre photometry in the home cage and during the visual discrimination task. See Supplementary Methods for a more detailed description. Fibre photometry was conducted as previously described[24,44]. For home-cage feeding, *ad libitum* fed mice were fasted for 24 h and then put in their home cage. We collected baseline data and then dropped a 0.2 g pellet into the home cage every 7–10 min. Fibre photometry during the visual discrimination task was performed using the same procedure described above for two-photon imaging of InsCtx.

Statistics. Statistical tests were performed using standard Matlab (MathWorks) functions. Differences across mice (for example, behaviour) were tested using a *t*-test because of relatively small sample sizes. Differences in neural activity across large populations of InsCtx neurons were tested using non-parametric tests (Kruskal–Wallis and Mann–Whitney tests) because of the non-normal distributions of the data. We did not assume equal/unequal variance in parametric *t*-tests, as all *t*-tests were paired.

Data analysis. All data analyses were performed using custom scripts in Matlab (MathWorks) and ImageJ (NIH). See Supplementary Methods for a more detailed description of the analyses described below.

Single-neuron response analyses. Initial image registration, time course extraction, and alignment of cell masks across runs and across days were performed as previously described[16]. Cells were then categorized as responsive to visual cues and/or licking and/or Ensure delivery, by independently testing evoked responses of each cell for each day the cell was identified. For visual cue responses, we compared mean 1-s pre-stimulus activity to activity in a 200-ms sliding window

from stimulus onset until 100 ms before licking onset, to minimize contamination by licking-related activity. We only compared time points that preceded licking onset by >100 ms in at least ten trials, using a Wilcoxon signed-rank test with a false discovery rate correction for multiple comparisons ($P < 0.05$). We also separately repeated this analysis using data up to 200 ms or 300 ms before licking onset and observed similar results (Extended Data Fig. 4a, b). We assessed a neuron's response magnitude using the maximal absolute value of the average cue response, and trial-to-trial variability using the Fano factor (variance/mean).

Pupil diameter and its effects on cue-evoked responses. To measure pupil diameter across hunger and satiety, we used pupil-tracking movies from both states acquired within the same imaging session. We concatenated data from 'Hungry' and 'Sated' sessions and performed all analyses on this concatenated movie. We warped and rotated the movie to achieve a circular pupil shape, and then used the Matlab function 'imfindcircles.m' to detect the pupil circumference in every frame separately, from which we extracted pupil diameter (scaled to correct for warping).

We calculated the average pre-cue pupil diameter in the 1-s interval before each cue during hunger and satiety. To identify pairs of trials with matched pupil diameter across states, we first searched for all 'satiety trials' with pre-cue diameter within ±10% of a 'hunger trial'. Of these, we then selected the 'satiety trial' that had the value nearest to the 'hunger trial' (matching ~50% of trials this way).

Orofacial movements and their effects on cue responses. We analysed orofacial movements as previously described[9]. We used the same procedure to analyse both licking-independent orofacial movements and neuronal cue responses (using only orofacial/neuronal data up to 100 ms before the first lick). We examined trial-to-trial variability in neuronal responses versus orofacial responses by calculating the Pearson correlation between the absolute value of neuronal response and orofacial response per trial (average of 0–1.5 s after cue onset), testing for a positive correlation coefficient.

Evaluation of spatial clustering of neurons with similar functional properties. We calculated pairwise distances between all neurons and examined the distribution of distances between neurons that were either similar or different in their responses type (food-cue-responsive versus licking/Ensure-responsive).

Comparisons across natural or artificial hunger states. We first aligned data from the 2 days of the experiment and only used neurons that were active and could be reliably identified on both days. We normalized the responses of each neuron within a day across states, using a single transformation (*z*-score) that was applied to all cue response trials. Z-scoring was performed by $(x_i - \bar{x})/S$, where x_i is $\Delta F/F$ at time-point i, $\bar{x}$ is the average $\Delta F/F$ of all visual cue data from that day (all time points, all trials, all visual cues, all states), and S is the standard deviation of $\Delta F/F$ from all visual cue presentations from that day (all time points, all trials, all visual cues, all states).

The 'hunger modulation index' was calculated for each neuron as $(R_{hungry} - R_{sated})/(R_{hungry} + R_{sated})$, where R is a neuron's average cue response, as described above. We assessed similarity across two given states using a three-step approach. First, we calculated a 'state modulation index' (similar to the hunger modulation index). Second, we compared the state modulation index with the similarity within-state of Hungry-1 by assessing each neuron's reliability (or 'self-similarity' in subsets of trials) by randomly splitting up trials into two halves and calculating the state modulation index between the two halves, repeated 100 times. Third, we compared the actual state modulation index across states/days to the neuron's 'self-similarity' and classified it as similar if (1) both state modulation indices (across-state and within-state) were between the 10th and 90th percentiles of the 'self-similarity' distribution and (2) both state modulation indices had the same sign (excitation/suppression).

Comparisons across saline and CNO injections during inhibition of BLA→InsCtx neurons. We first aligned data from the 2 days, as described above. For subsequent analyses, we included all neurons that were cue- and/or Ensure-responsive either on Saline-1.1 and/or on Saline-2.1. To facilitate comparisons across experimental conditions, we used the same within-day *z*-scoring procedure described above. The 'modulation index' was calculated for each neuron per day as $(R_{session 2} - R_{session 1})/(R_{session 2} + R_{session 1})$, where R is a neuron's average cue response, as described above.

Population decoding. For each mouse and session, we used all simultaneously imaged neurons. We used within-day, across-state, *z*-scored time courses of responses to each cue, re-zeroed using the 1-s pre-cue period. For each trial, we then obtained a population 'template vector' for each cue by calculating the average cue-evoked response per neuron and normalized it to obtain a vector of unit magnitude so as to classify only on the basis of the pattern (not magnitude) of population responses. For each trial, we obtained a 'single-trial vector' that was also normalized to unit magnitude. We then calculated the cosine similarity between 'trial vectors' and 'template vectors' for each cue. The decoder's prediction of which cue was presented during that trial was the cue whose 'template vector' was most similar to the 'trial vector' (highest cosine similarity). Decoder accuracy was the fraction of food cue trials with a correct prediction of food cue presentation (chance: 33%). We assessed maximal decoder accuracy by creating

a 'template vector' from a randomly selected subset of 75% of trials for each cue, and tested the decoder on the remaining 25%. This was repeated 1,000 times, and the average of these repetitions was used as maximal decoding accuracy. Of note, while we intentionally used a simple linear decoder, nonlinear decoders might achieve higher accuracy.

Fibre photometry data analysis. Traces were downsampled from 1 kHz to 100 Hz and smoothed using a 1-s running average. We calculated $\Delta F/F = (F - F_0)/F_0$. In home-cage pellet drop experiments, F_0 was the average of 30 s before the first pellet drop. In the visual discrimination task, F_0 was the average of 1 s before each cue.

Data availability. The original and/or analysed data sets generated during the current study, and the code used to analyse them, are available from the corresponding authors on reasonable request.

44. Garfield, A. S. et al. Dynamic GABAergic afferent modulation of AgRP neurons. *Nat. Neurosci.* **19,** 1628–1635 (2016).
45. Petreanu, L. et al. Activity in motor-sensory projections reveals distributed coding in somatosensation. *Nature* **489,** 299–303 (2012).
46. Chen, T. W. et al. Ultrasensitive fluorescent proteins for imaging neuronal activity. *Nature* **499,** 295–300 (2013).
47. Aronoff, R. et al. Long-range connectivity of mouse primary somatosensory barrel cortex. *Eur. J. Neurosci.* **31,** 2221–2233 (2010).
48. Wickersham, I. R. et al. Monosynaptic restriction of transsynaptic tracing from single, genetically targeted neurons. *Neuron* **53,** 639–647 (2007).
49. Atasoy, D. et al. A genetically specified connectomics approach applied to long-range feeding regulatory circuits. *Nat. Neurosci.* **17,** 1830–1839 (2014).
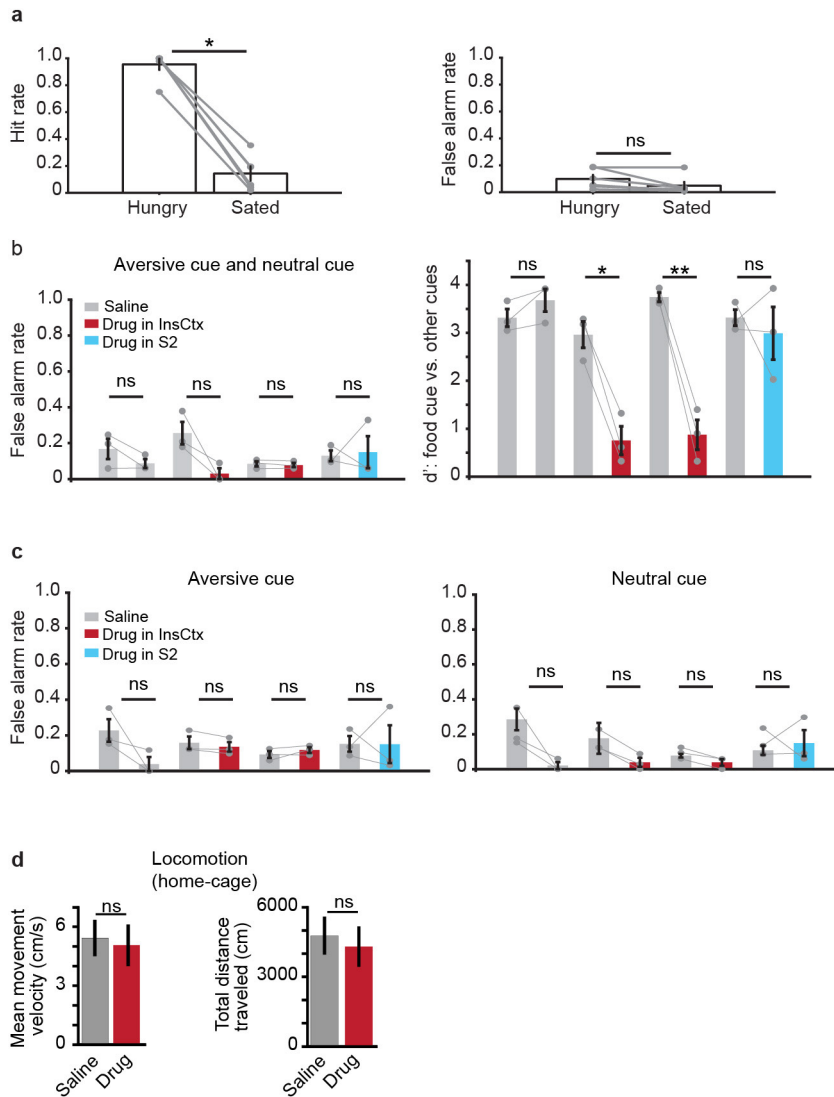
Extended Data Figure 1 | Behaviour during hunger, satiety, and InsCtx silencing. a, Summary of task performance across mice, during hunger and satiety. Hit rate: fraction of food cue trials with correct behavioural response (licking within the 2 s response window after cue offset). False alarm rate: fraction of non-food-cue trials in which mice incorrectly licked within the 2 s response window after cue offset. Each dot represents one mouse; lines connect two same-day blocks from the same mouse. *$P = 1.8 \times 10^{-5}$, NS, not significant ($P = 0.09$); paired t-test, $n = 6$ mice. Mean ± s.e.m. **b,** Summary of task performance after InsCtx silencing in hungry mice: false alarm rate and d' (sensitivity index, which combines hit rate and false alarm rate in a general measure of discrimination), combining both aversive cue and neutral cue trials. Each dot represents one mouse; lines connect two same-session blocks of trials from the same mouse (first day: block 1, saline; block 2, saline; all other days: block 1, saline; block 2, drug). Notice that pharmacological silencing of InsCtx, but not of secondary somatosensory cortex (S2), reduces performance in the visual discrimination task (d') because of reduced hit rates (Fig. 1c), without significantly affecting false alarm rates. Bars and error bars, mean ± s.e.m.; NS, not significant ($P \geq 0.2$); *$P = 0.01$; **$P = 0.007$; paired t-test, $n = 3$ mice. Mean ± s.e.m. **c,** False alarm rates for aversive cues trials (left) and neutral cue trials (right). Each dot represents one mouse; lines connect two same-session blocks of trials from the same mouse (first day: block 1, saline; block 2, saline; all other days: block 1, saline; block 2, drug). Notice that pharmacological silencing of InsCtx did not significantly affect false alarm rates for aversive cue trials or for neutral cue trials. NS, not significant ($P \geq 0.06$); paired t-test, $n = 3$ mice. Mean ± s.e.m. **d,** Movement velocity and total distance travelled in the home cage after saline or drug infusion into InsCtx. Note that pharmacological silencing of InsCtx did not affect general locomotion in the home cage. NS, not significant ($P \geq 0.34$); paired t-test, $n = 3$ mice. Mean ± s.e.m.
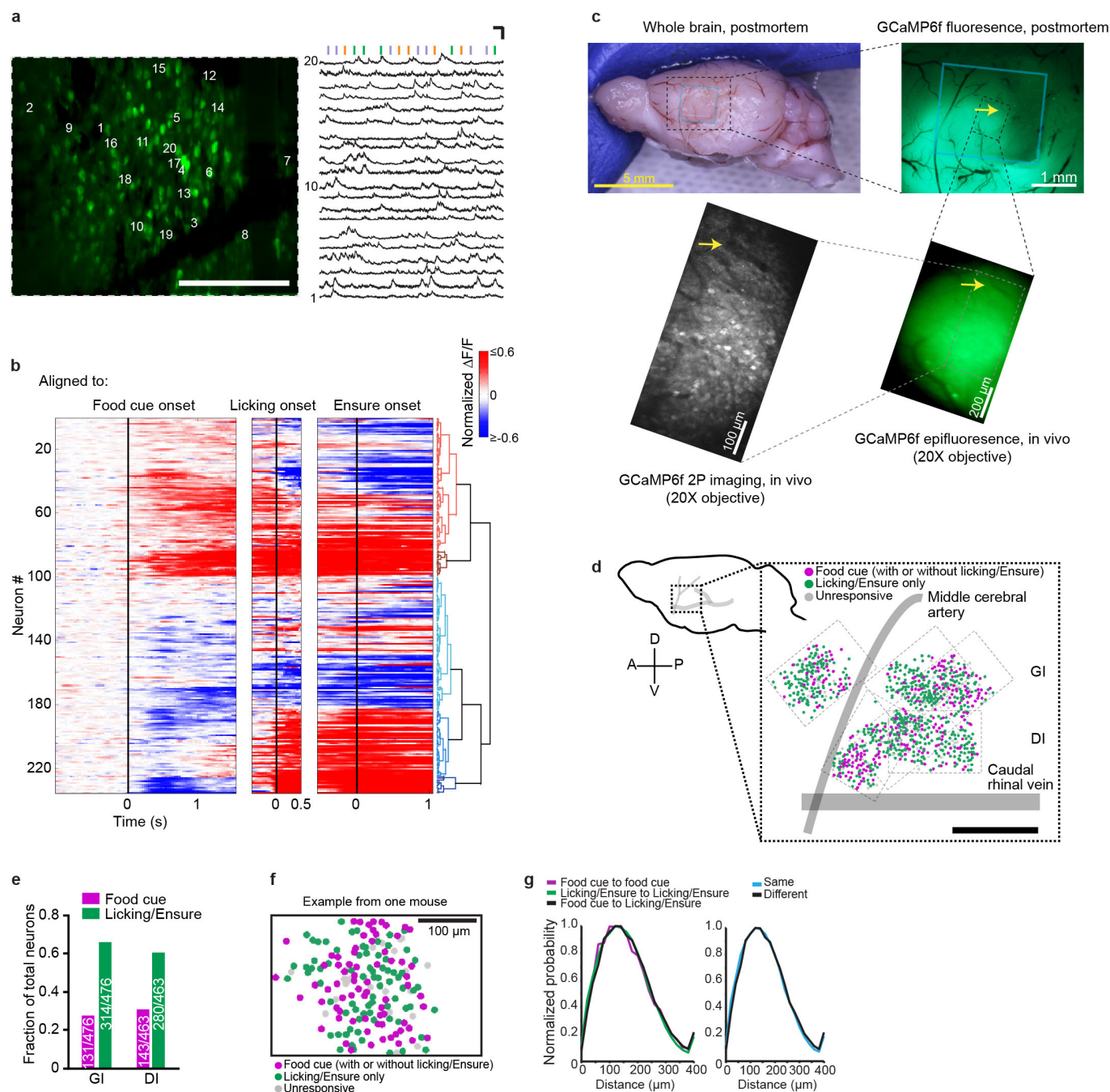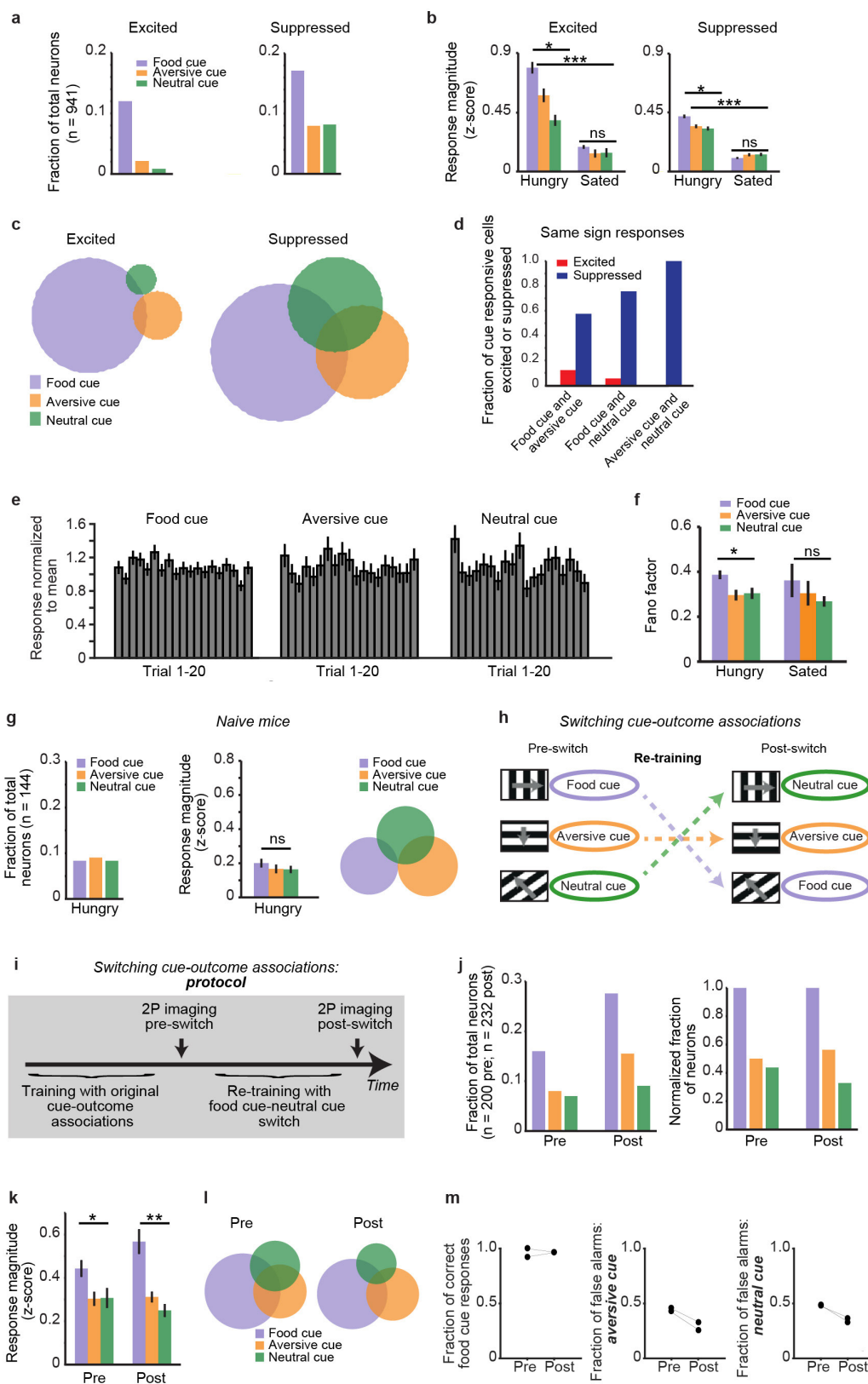
Extended Data Figure 2 | See next page for caption.

Extended Data Figure 2 | InsCtx activity from an example field of view; most food-cue-responsive neurons also respond to licking/Ensure; localizing imaging fields of view relative to vasculature; no spatial organization of InsCtx food cue and licking/Ensure responses.
a, Example two-photon image (same mouse as in Fig. 1f) containing ~150 active neurons. Scale bar, 100 μm. Right: example activity of 20 neurons (labelled in the left panel) from the same field of view during the behavioural task (vertical bars: presentation of visual cues). Scale bars, 10 s and 100% ($\Delta F/F$). Note that GCaMP dynamics reflect the high ongoing firing rates of mouse InsCtx neurons *in vivo* (6–10 Hz on average; ref. 10). **b**, Heatmaps of average responses of all food-cue-responsive neurons meeting the criteria for the clustering analysis (each row is the average activity of a single neuron). Neurons were clustered on the basis of their food cue and licking responses (see Methods). Different heatmaps were aligned to different events (food cue onset, licking onset, Ensure delivery), and all responses were computed relative to the pre-cue period. Notice that many food-cue-responsive neurons also responded to licking/Ensure. **c**, Post-mortem analysis of the location of the microprism and imaging field of view. Top left: side-view image of the brain of a mouse implanted with a microprism. Blue rectangle shows location of microprism imaging face, identified by a minor indentation of the brain. Top right: post-mortem epifluorescence image of GCaMP6f in lateral cortex. Blue rectangle shows microprism location. Bottom right: *in vivo* epifluorescence image of GCaMP6f through the microprism at the imaging field of view location. Bottom left: *in vivo* two-photon field of

view, imaged through the microprism. The image was adjusted to enhance the visibility of the neuropil and vasculature. Arrows point to the same vascular landmark in different images. **d**, Left: schematic side view of the mouse brain. Right: anatomical location of all imaged neurons (dots) across mice, relative to the junction of caudal rhinal vein and middle cerebral artery. Magenta: food-cue-responsive neurons; green: licking and/or Ensure-responsive neurons; grey: unresponsive neurons; dashed rectangles: borders of each imaging field. Scale bar, 0.5 mm. **e**, Fraction of food-cue-responsive neurons and of licking and/or Ensure-responsive neurons in granular (GI) versus dysgranular (DI) subregions of InsCtx. **f**, Example field of view from one mouse. Neuron locations are marked with coloured circles (magenta: food-cue-responsive; green: licking/Ensure-responsive only; grey: unresponsive). Scale bar, 100 μm. **g**, Left: distribution of distances between pairs of neurons in which (1) both neurons were responsive to the food cue (magenta), (2) both neurons were responsive to licking/Ensure (green), and (3) one neuron was responsive to the food cue and the other neuron is responsive to licking/Ensure (black). Note that all three distributions are similar, suggesting no spatial clustering. Right: distribution of distances between pairs of neurons having the same type of response (that is, either both responding to the food cue or both responding to licking/Ensure, blue), and between pairs of neurons with different response types (for example, one neuron responding to the food cue and the other responding to licking/Ensure, black). Note that these distributions are similar, suggesting no spatial clustering.
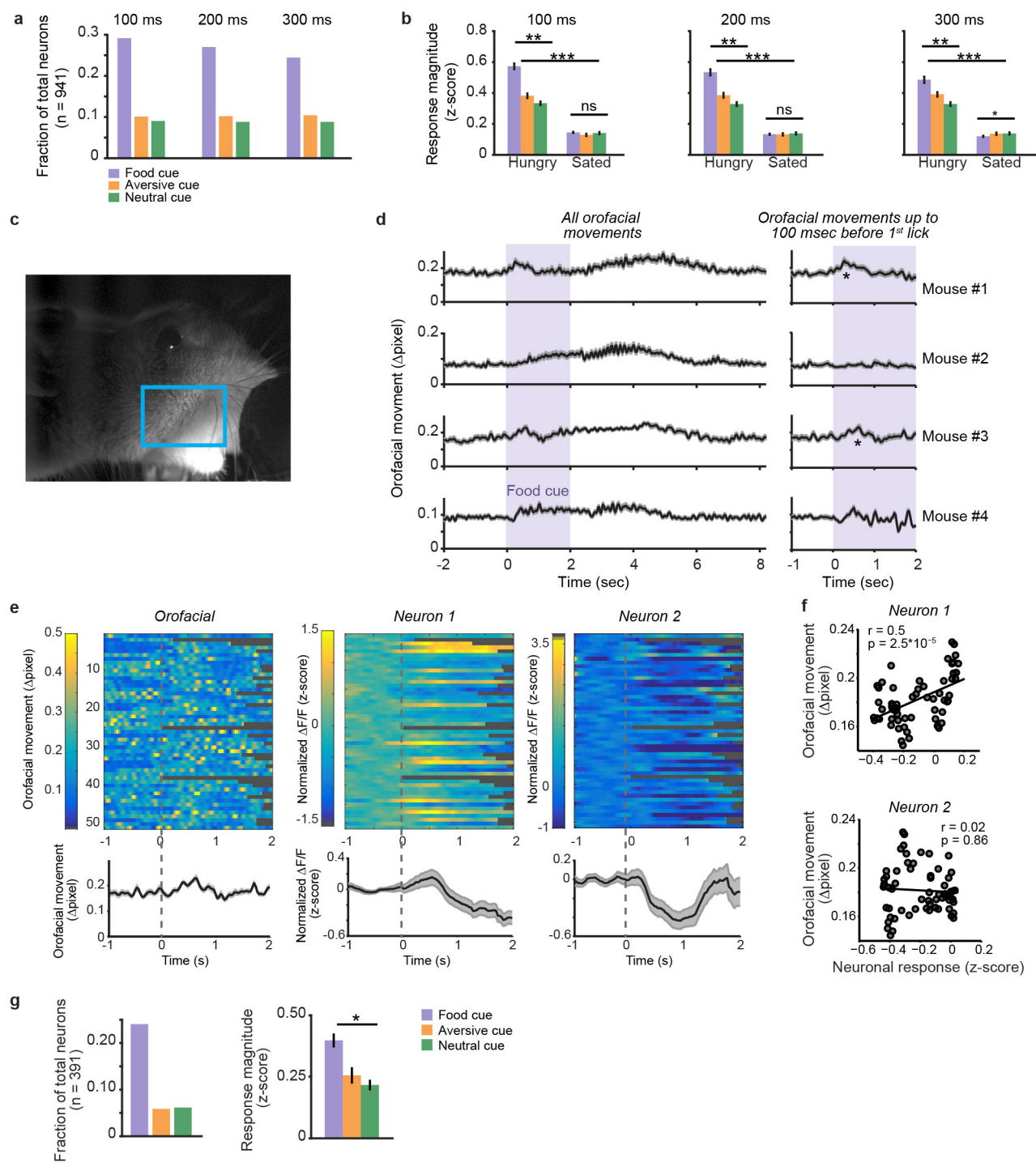
Extended Data Figure 3 | See next page for caption.

Extended Data Figure 3 | Further analyses of InsCtx cue responses; InsCtx food cue bias emerges after learning and is not dependent on cue orientation or on overexposure to the food cue during early training.
a, Separate analysis of the fraction of cue-responsive neurons for neurons that were either excited (left) or suppressed (right) by cue presentation. Note the stronger food cue bias in neurons with cue-evoked excitation. **b**, Separate analysis of the response magnitude in excited and suppressed neurons, across hunger and satiety. Note the stronger food cue bias in excited neurons, but no food cue bias during satiety in both groups. Also, note that the responses to the aversive and neutral cues are significantly different only in excited neurons. Excited: *$P = 0.002$ (Hungry); NS, not significant ($P = 0.3$, Sated); Kruskal–Wallis test. Pairwise comparisons (Hungry): food cue versus aversive cue, $P = 0.04$; food cue versus neutral cue, $P = 0.003$; aversive cue versus neutral cue, $P = 0.02$. Pairwise comparisons (Hungry versus Sated): ***$P \leq 6 \times 10^{-4}$ for all three cues; Mann–Whitney U-test ($n = 113$, 20, and 8 neurons responding to the food, aversive, and neutral cues, respectively; from six mice). Suppressed: *$P = 2.4 \times 10^{-5}$ (Hungry); NS, not significant ($P = 0.2$, Sated); Kruskal–Wallis test. Pairwise comparisons (Hungry): food cue versus aversive cue, $P = 8.3 \times 10^{-4}$; food cue versus neutral cue, $P = 5.6 \times 10^{-5}$; aversive cue versus neutral cue, $P = 0.3$. Pairwise comparisons (Hungry versus Sated): ***$P \leq 7 \times 10^{-17}$ for all three cues; Mann–Whitney U-test ($n = 171$, 75, and 77 neurons responding to the food, aversive, and neutral cues, respectively; from six mice). Mean ± s.e.m. **c**, Separate analysis of the cue response selectivity of neurons that were excited or suppressed by cue presentation. Each circle represents all excited/suppressed neurons that were responsive to a given visual cue. Note the higher selectivity in excited neurons. See **b** for sample sizes. **d**, Analysis of the response sign (excited/suppressed) of neurons that significantly responded to two cues. Fraction of neurons that significantly responded with the same sign to two different cues, out of the total neurons that responded to the two cues with the same or opposite sign (for example: red, number of neurons excited by food cue and aversive cue out of all neurons excited by the food cue and either excited or suppressed by aversive cue; blue, number of neurons suppressed by food cue and aversive cue out of all neurons suppressed by the food cue and either excited or suppressed by aversive cue). Note that only a very small fraction of neurons excited by the food cue were also excited by one of the other two cues (that is, they were suppressed by the other two cues). Also, note that a substantial fraction of neurons significantly suppressed by one cue would also be suppressed by one or more other cues. **e**, Analysis of average responses across all neurons for each of the first 20 presentations of each cue within a session. For each neuron with a significant response to a given cue, cue responses were normalized by their mean across the session. These normalized cue responses were then averaged across neurons per trial. Note that, at the population level, cue responses did not show substantial differences between early and later trials. Mean ± s.e.m. **f**, Fano factor as a measure of trial-to-trial cue response variability across states. Note that, during hunger but not during satiety, the Fano factor was significantly higher for responses to the food cue than for responses to the other two cues. *$P = 0.01$ (Hungry); NS, not significant ($P = 0.4$, Sated); Kruskal–Wallis test. Pairwise comparisons (Hungry): food cue versus aversive cue, $P = 0.007$; food cue versus neutral cue, $P = 0.04$; aversive cue versus neutral cue, $P = 0.7$. Pairwise comparisons (Hungry versus

Sated): $P = 2 \times 10^{-5}$ for the food cue; $P = 0.2$ for the aversive and neutral cues; Mann–Whitney U-test ($n = 274$, 95, and 85 neurons responding to the food, aversive, and neutral cues, respectively; from six mice). Mean ± s.e.m. **g**, No food cue bias before learning. Fraction of responsive neurons (left), response magnitude (middle), and response selectivity (right) in naive mice before learning the visual discrimination task. Mice were imaged while in a hungry state (85% *ad libitum* body weight). Note that there was no food cue bias in the fraction of responsive neurons ($n = 144$ neurons from three mice), nor in response magnitude, and that selectivity was relatively high. NS, not significant ($P = 0.4$); Kruskal–Wallis test ($n = 12$, 13, and 12 neurons responding to the food, aversive, and neutral cues, respectively; from three mice). Mean ± s.e.m. Note also the relatively low responsiveness and response magnitude compared with well-trained mice (compare, for example, **k** below). **h–m**, To test whether InsCtx food cue bias was dependent on the actual cue orientation or on overexposure to the food cue during early training (see Methods), we switched cue–outcome associations. First, we trained mice in the usual cue–outcome associations and imaged InsCtx to verify food cue bias. We then switched the food cue and neutral cue, and exposed mice to the same number of repetitions of each cue during re-training. We then imaged InsCtx in the same mice again to test whether there was a bias to the new food cue (that is, to the visual grating orientation that now predicted food but that formerly predicted no outcome). **h**, Schematic of cue–outcome associations in the initial training and then after the food-cue-neutral cue switch. Importantly, in all subsequent analyses, we refer to the Ensure-rewarded cue as the 'food cue' regardless of its actual visual grating orientation. **i**, Experimental protocol of switching cue–outcome associations. **j**, Fraction of responsive neurons to each cue before and after the food-cue-neutral cue switch. Left: fraction of all imaged neurons before and after ($n = 200$ pre, $n = 232$ post; from two mice). Note that after the switch, the overall fraction of responsive neurons to all cues increased, potentially because of increased GCaMP6f expression over time. Right: fraction of all imaged neurons before and after, normalized to the fraction of food-cue-responsive neurons to demonstrate a similar relative level of food cue bias. **k**, Average response magnitude before and after the food-cue-neutral cue switch. Note the food cue response bias both before and after the switch. *$P = 0.01$ (pre); **$P = 1.4 \times 10^{-5}$ (post); Kruskal–Wallis test. Pairwise comparisons were as follows. Pre, food cue versus aversive cue, $P = 0.01$; food cue versus neutral cue, $P = 0.02$; aversive cue versus neutral cue, $P = 0.9$; Mann–Whitney U-test ($n = 32$, 16, and 14 neurons responding to the food, aversive, and neutral cues, respectively; from two mice). Post: food cue versus aversive cue, $P = 2.9 \times 10^{-4}$; food cue versus neutral cue, $P = 8.9 \times 10^{-5}$; aversive cue versus neutral cue, $P = 0.2$; Mann–Whitney U-test ($n = 64$, 36, and 21 neurons responding to the food, aversive, and neutral cues, respectively; from two mice). Mean ± s.e.m. **l**, Cue response selectivity of cue-responsive neurons before and after the food-cue-neutral cue switch. Circles represent number of neurons responsive to a given visual cue. Note the higher cue selectivity of food-cue-responsive neurons both before and after the food-cue-neutral cue switch. **m**, Behavioural performance of the visual discrimination task before and after switching cue–outcome associations ($n = 2$ mice). Each dot is data from a single mouse, and lines connect the same mice before and after the switch.

Extended Data Figure 4 | See next page for caption.

Extended Data Figure 4 | InsCtx food cue bias and hunger modulation cannot be explained by licking or other orofacial movements.
**a**, **b**, Analysis of cue responses before licking onset. All cue response analyses presented in all figures were performed by analysing data up to 100 ms before the first lick on each trial (see Methods). Here we increased this period to 200 ms and to 300 ms, and demonstrated that food cue bias and hunger modulation persisted and were thus independent of licking. **a**, Analysis of the fraction of cue-responsive neurons for response epochs from cue onset to either 100 ms, 200 ms, or 300 ms before onset of the first lick. Note a similar food cue bias across analyses. **b**, Average response magnitude across hunger and satiety for the response epochs described above. Note the response bias to the food cue decreased slightly for analyses restricted to 200 ms and 300 ms before the first lick, but was still prominent and was consistently abolished after satiation. One hundred milliseconds: **$P = 2.8 \times 10^{-12}$ (Hungry); NS, not significant ($P = 0.6$, Sated); Kruskal–Wallis test. Pairwise comparisons (Hungry): food cue versus aversive cue, $P = 1.7 \times 10^{-8}$; food cue versus neutral cue, $P = 7.3 \times 10^{-11}$; aversive cue versus neutral cue, $P = 0.01$. Pairwise comparisons (Hungry versus Sated): ***$P \le 2.7 \times 10^{-19}$ for all three cues; Mann–Whitney U-test ($n = 274$, 95, and 85 neurons responding to the food, aversive, and neutral cues, respectively; from six mice). Two hundred milliseconds: **$P = 1.5 \times 10^{-8}$ (Hungry); NS, not significant ($P = 0.5$, Sated); Kruskal–Wallis test. Pairwise comparisons (Hungry): food cue versus aversive cue, $P = 1.8 \times 10^{-4}$; food cue versus neutral cue, $P = 6.7 \times 10^{-8}$; aversive cue versus neutral cue, $P = 0.04$. Pairwise comparisons (Hungry versus Sated): ***$P \le 1.9 \times 10^{-17}$ for all three cues; Mann–Whitney U-test ($n = 274$, 95, and 85 neurons responding to the food, aversive, and neutral cues, respectively; from six mice). Three hundred milliseconds: **$P = 0.0003$ (Hungry); *$P = 0.01$ (Sated); Kruskal–Wallis test. Pairwise comparisons (Hungry): food cue versus aversive cue, $P = 0.04$; food cue versus neutral cue: $P = 1.7 \times 10^{-4}$; aversive cue versus neutral cue, $P = 0.03$. Pairwise comparisons (Hungry versus Sated): ***$P \le 1.7 \times 10^{-17}$ for all three cues; Mann–Whitney U-test ($n = 274$, 95, and 85 neurons responding to the food, aversive, and neutral cues, respectively; from six mice). Mean ± s.e.m. **c**–**g**, Analysis of orofacial movements and their potential effect on InsCtx food cue response bias. **c**, Image of the face of a mouse performing the behavioural task during imaging of InsCtx. Blue rectangle marks the region of interest analysed

for orofacial movements (see Methods). **d**, Orofacial movements in four mice. Left: average across food cue trials of all orofacial movements. Right: average across food cue trials of orofacial movements up to 100 ms before the first lick in each trial (same procedure used to analyse licking-independent cue responses in InsCtx, see **a** and **b** above). Only mouse 1 and mouse 3 had significant licking-independent orofacial movements. Mean ± s.e.m. **e**, Examples of simultaneous recordings of orofacial movements (left) and activity of two neurons (middle and right) from mouse 3. Top: heatmaps of neuronal activity and orofacial movements. Note that for every trial, data were analysed up to 100 ms before the first lick, and all subsequent data points (that is, not analysed for cue responses) are coloured in grey. Bottom: average across trials, mean ± s.e.m. **f**, Correlation between orofacial movements and single-trial neuronal responses for the two neurons in **e**. Note that responses in neuron 1 were positively correlated with orofacial movements, while responses in neuron 2 were not correlated with orofacial movements. Orofacial responses have been shown to drive some InsCtx neurons. If food cue responses were caused by orofacial responses, this would be reflected by a positive correlation between neuronal responses and orofacial movements. However, only 3% of food-cue-responsive neurons were positively correlated with orofacial movements across trials ($n = 94$, from four mice; different mice from those in Fig. 2). This suggests that with our analyses (that is, analysing activity up to 100 ms before the first lick at each trial), orofacial movements do not contribute to food cue responses or to the food cue bias in InsCtx (see **g**). **g**, Food cue bias in InsCtx neurons from this separate cohort of four mice, most of which lacked a positive correlation between food cue responses and orofacial movements. Left: fraction of neurons responsive to each cue, from all experiments in which neurons were imaged during simultaneous tracking of orofacial movements. Note the food cue bias. Right: average response magnitude from neurons imaged while also acquiring orofacial movements. Note that the response bias to the food cue is similar to that in Fig. 2. *$P = 2.8 \times 10^{-5}$, Kruskal–Wallis test. Pairwise comparisons: food cue versus aversive cue, $P = 0.003$; food cue versus neutral cue: $P = 5.9 \times 10^{-5}$; aversive cue versus neutral cue, $P = 0.45$; Mann–Whitney U-test ($n = 94$, 23, and 24 neurons responding to the food, aversive, and neutral cues, respectively; from four mice). Mean ± s.e.m.
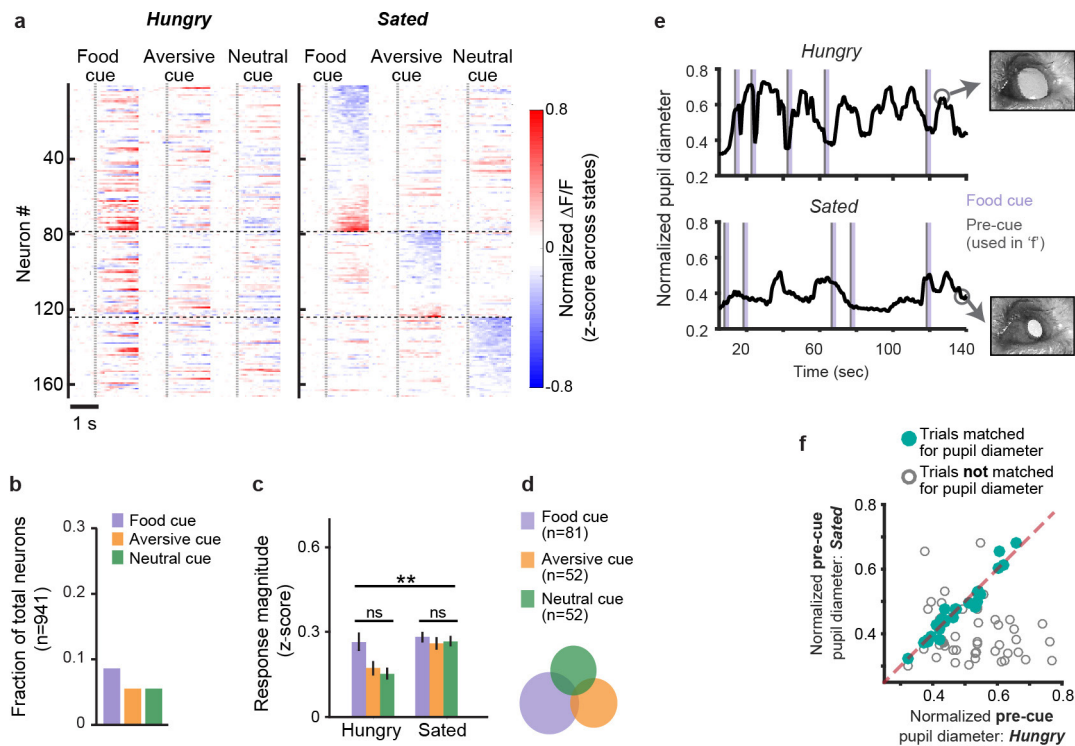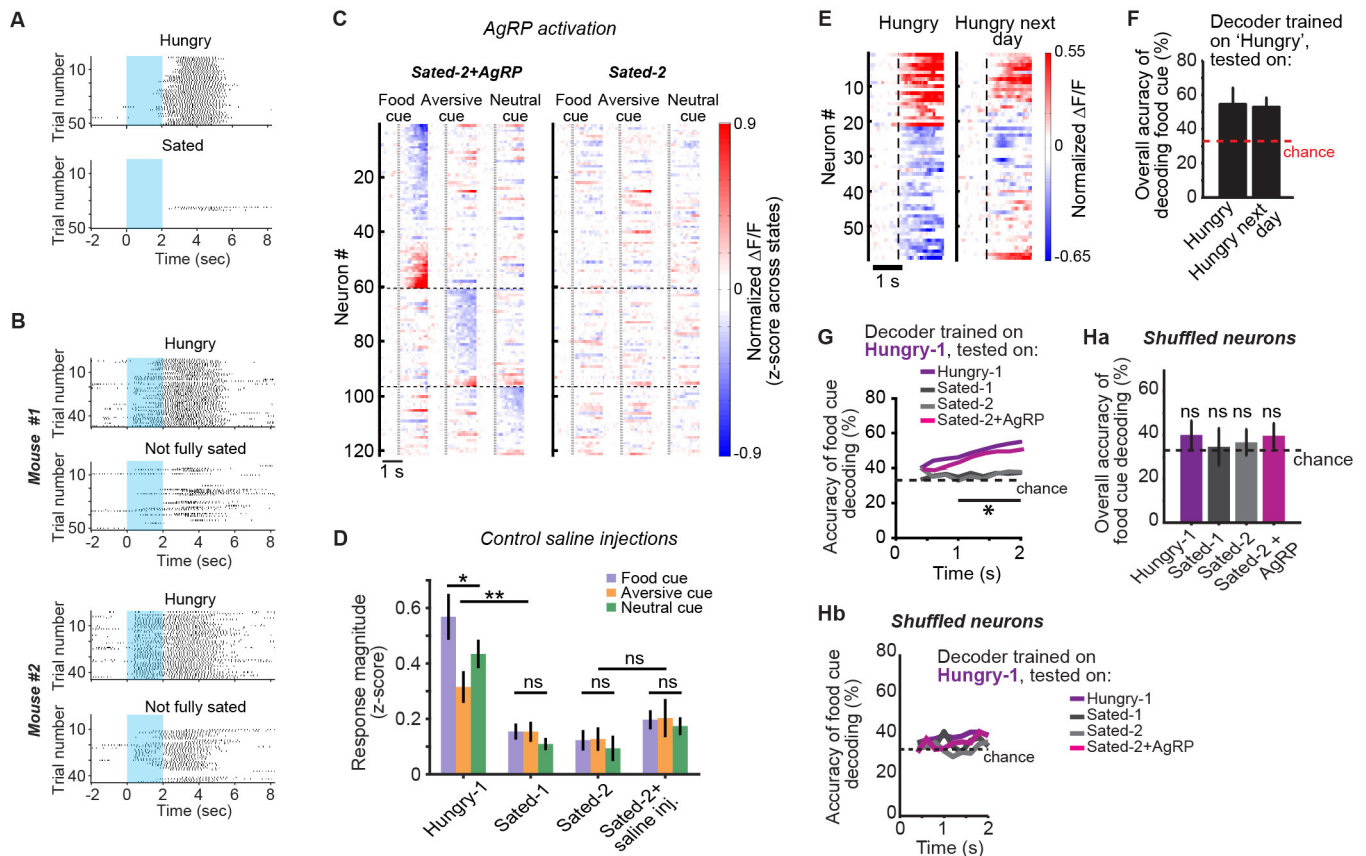
Extended Data Figure 5 | A subset of InsCtx neurons respond to visual cues during satiety; using pre-cue pupil diameter to match trials for similar arousal levels across states. a, Heatmap of the average neuronal responses to the three visual cues during hunger and satiety for all neurons that were significantly cue-responsive during satiety. **b**, Fraction of neurons significantly responsive to each cue during satiety (out of 941 recorded neurons from six mice). **c**, Response magnitude across hunger and satiety in neurons with significant cue responses in the sated state. Note the absence of a significant response bias to the food cue during hunger or satiety in this set of neurons. NS, not significant; $P = 0.09$ (Hungry); $P = 0.59$ (Sated); Kruskal–Wallis test ($n = 166$ neurons from six mice). Pairwise comparisons (Hungry versus Sated): $**P \leq 0.002$

for all three cues; Mann–Whitney U-test ($n = 274$ neurons from six mice). Mean $\pm$ s.e.m. **d**, Selectivity of cue-responsive neurons. Each circle represents all neurons responding to a specific visual cue. Note that neurons responding to any one of the three cues displayed similar response selectivity. **e**, Pupil diameter dynamics during the discrimination task across hunger (top) and satiety (bottom). Images: examples of a dilated (top) and constricted (bottom) pupil. Grey and purple bars: pre-cue and cue periods, respectively. Same plot shown in Fig. 2. **f**, Pre-cue pupil diameters across single hungry and sated trials (same mouse from **e**), demonstrating the procedure for matching trials for similar pre-cue pupil diameters across states (see Methods). Line of unity, dashed pink.
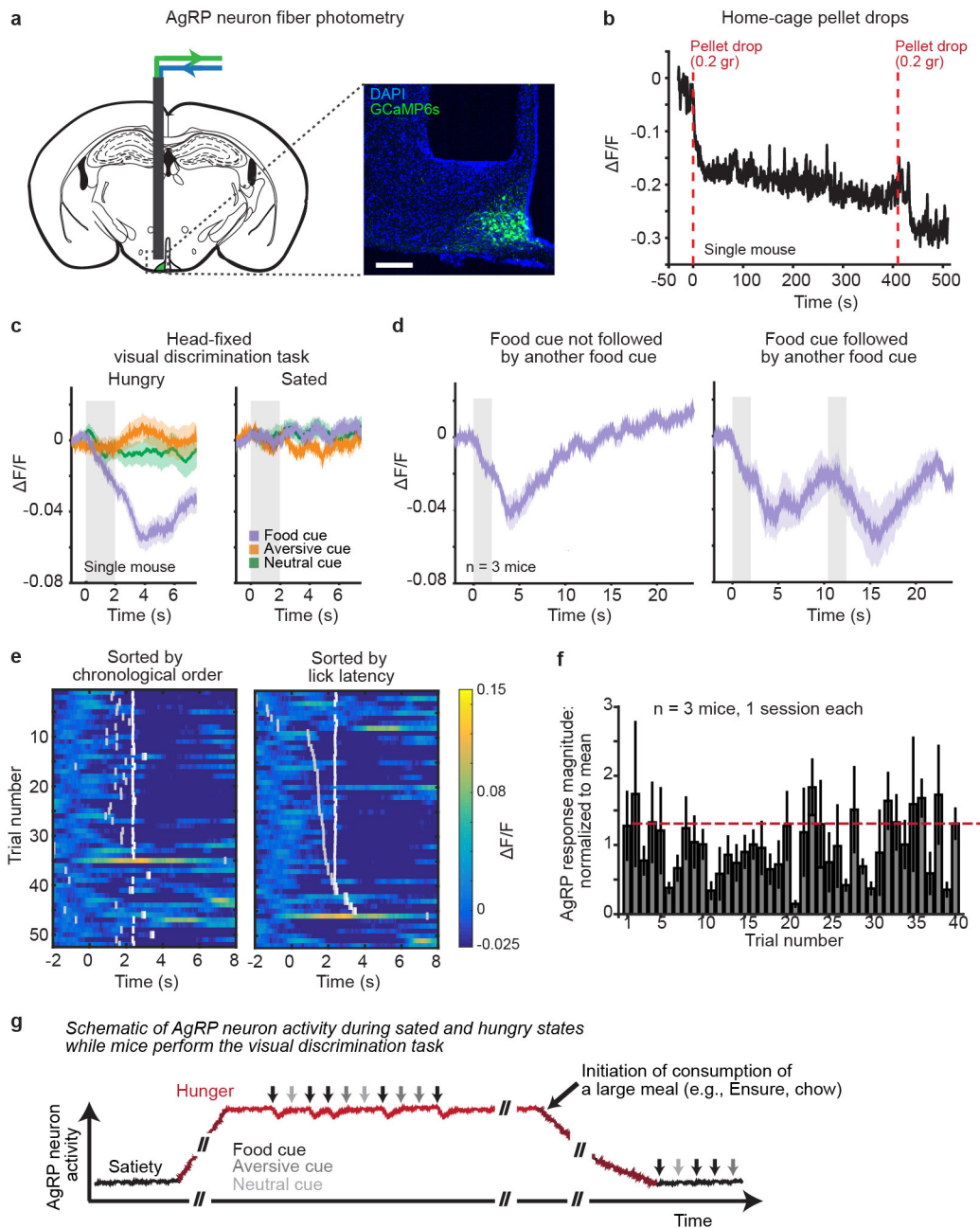
Extended Data Figure 6 | Persistent AgRP neuron food cue responses during performance of the visual discrimination task. a, AgRP neuron fibre photometry. Left: schematic of the fibre photometry approach. Right: image of GCaMP6s-expressing AgRP neurons in the ARC, with the fibre track above. Scale bar, 200 μm. **b**, Example photometry signal from one food-restricted mouse (same mouse in **a**) in response to delivery of two small food pellets (0.2 g each). Note an acute decrease in AgRP activity in response to the first pellet, and a subsequent, additional acute decrease after the second pellet, demonstrating that AgRP activity was not completely inhibited after delivery of the first pellet. **c**, Average cue responses in the visual discrimination task during hunger and satiety, from the same mouse as in **b**. Note that in the hungry state, AgRP neurons responded to the food cue, but not to the other cues. During the sated state, AgRP neurons were not responsive to any cue. Values are mean ± s.e.m. across 50–55 trials per cue. Shaded region: cue duration. **d**, AgRP neuron responses to food cues either followed (right) or not followed (left) by another food cue (cues were presented with an interval of 8–10 s, see Methods). Note that AgRP neuron activity returned to baseline levels after each food cue that was not followed by another food cue (but it was followed by either another cue that did not elicit a response or by a blank trial, see Methods). Furthermore, AgRP neurons responded similarly to another presentation of a food cue, spaced 8–10 s

apart. Values are mean ± s.e.m. across three mice. Shaded region: food cue duration. **e**, Heatmaps of food cue responses (same mouse in **a**–**c**) across single trials, sorted chronologically (left) or by licking latency (right). Grey and white tick marks show licking onset and Ensure delivery, respectively. Note that there was substantial trial-to-trial variability in food cue responses that could not be explained by trial recency or by licking behaviour. **f**, Analysis of responses to each of the first 40 presentations of the food cue within a session, averaged across one session from each of three mice. Cue responses were normalized by their mean across the session. These normalized cue responses were then averaged across mice. Dashed red line, normalized response to the first cue presentation. Note that cue responses did not show substantial differences between early and later trials. Values are mean ± s.e.m. **g**, Schematic of AgRP neuron activity during satiety, the visual discrimination task, and subsequent satiation, on the basis of the experiments in **a**–**f**. AgRP neuron activity remained high (relative to satiety) in food-restricted mice during the visual discrimination task, and dropped only transiently after every food cue and consumption of a very small amount of Ensure (5 μl). Satiation (via consumption of either Ensure or chow) reduced the activity of AgRP neurons to lower levels and eliminated subsequent neuronal responses to food cue presentation. Black, dark grey, and light grey arrows: food cue, aversive cue, and neutral cue.

Extended Data Figure 7 | Satiation by consumption of Ensure can be labile; InsCtx neuronal responses to the three visual cues during Sated-2 + AgRP and Sated-2; saline injections do not mimic hunger in InsCtx; comparison of InsCtx responses in hungry mice across two daily sessions; time course of decoding accuracy and the necessity of neuronal identity for decoding accuracy. A, Example licking raster plots from a single session, for food cue trials presented during hunger and satiety. Intermingled aversive and neutral cue presentations are omitted for clarity. Note cue-evoked licking during hunger but not during satiety. **B**, Examples licking raster plots from two mice, for a session in which each mouse was not fully sated and thus partly re-engaged in the task for a substantial number of trials after initial satiation. Note that in such cases we stopped the experiment, and re-sated the mice with delivery of additional Ensure until they were fully sated (operationally defined as lack of voluntary licking for Ensure, see Methods). **C**, Heatmap of the average response to the three visual cues during Sated-2 + AgRP and Sated-2 for each neuron (one row per neuron) that was significantly responsive to at least one cue during Sated-2 + AgRP. Vertical dashed lines: visual cue onset. Horizontal dashed lines: grouping of neurons by the cue that evoked the strongest response. **D**, Saline injections did not mimic hunger in InsCtx. Average response magnitude of InsCtx neurons across hunger, satiety, and saline injections ($n = 109$ neurons from two mice, different mice from those in **c**). *$P = 0.03$ (Hungry); NS, not significant ($P \geq 0.5$, Sated-1, Sated-2, Sated-2 + saline injections); Kruskal–Wallis test. Pairwise comparisons across states (Hungry-1 versus Sated-1): food cue, $P = 2.4 \times 10^{-5}$; aversive cue, $P = 0.02$; neutral cue, $P = 1.7 \times 10^{-5}$. Pairwise comparisons across states (Sated-2 versus Sated-2 + saline injections): $P \geq 0.15$ for all three cues; **$P < 0.02$; NS, not significant; Mann–Whitney U-test. Mean ± s.e.m. Note the population response bias to the food cue in Hungry-1, but not in Sated-2 + saline injections. Furthermore, while there was a food cue bias in the fraction of responsive neurons per cue during

hunger (Hungry-1; food cue, 0.16; aversive cue, 0.10; neutral cue, 0.12), saline injections in sated mice did not induce a similar food cue bias ('Sated-2 + saline inj.'; food cue, 0.05; aversive cue, 0.07; neutral cue, 0.05; $n = 109$ neurons from two mice). **E**, Heatmap of all food-cue-responsive neurons during two consecutive imaging sessions, both performed while the mice ($n = 4$) were hungry. Note that some neurons were similarly responsive on both days, while others were not. **F**, Average decoding accuracy. The decoder was trained on data from entire populations of neurons recorded during the first 'Hungry' session, and tested on other 'Hungry' data from the same neurons on the same day, or from the same neurons recorded on the following day ('Hungry-next-day' data; $n = 4$ mice). Note that decoding accuracy was similar. **G**, Average time course of accuracy of population decoding of whether a food cue was presented versus other cues (see text for details). *All time points that were significantly different from chance (33%) for 'Sated-2 + AgRP stim.' ($P \leq 0.03$, paired t-test, Holm–Bonferroni correction for multiple comparisons, $n = 4$ mice). Decoding was performed on single-trial responses of simultaneously imaged ensembles (90–98 neurons per mouse, $n = 4$ mice). **H**, **a**, Overall food cue decoding accuracy after shuffling of neuronal identity. Data are averages of 100 shuffles for each mouse separately ($n = 4$ mice). Note that shuffling neuronal identity decreased overall decoding accuracy to chance levels. All values are mean ± s.e.m. across mice. **H**, **b**, Average time course of accuracy of decoding the food cue versus other cues, after shuffling of neuronal identity (see text for details). Data are averages of 100 shuffles, performed separately for each mouse ($n = 4$ mice). Note that shuffling neuronal identity decreased decoding accuracy to chance levels, and that decoding accuracy did not increase with time. Thus, decoding accuracy stemmed from the specific pattern of responses across the population and not from global biases in response strength or response type.
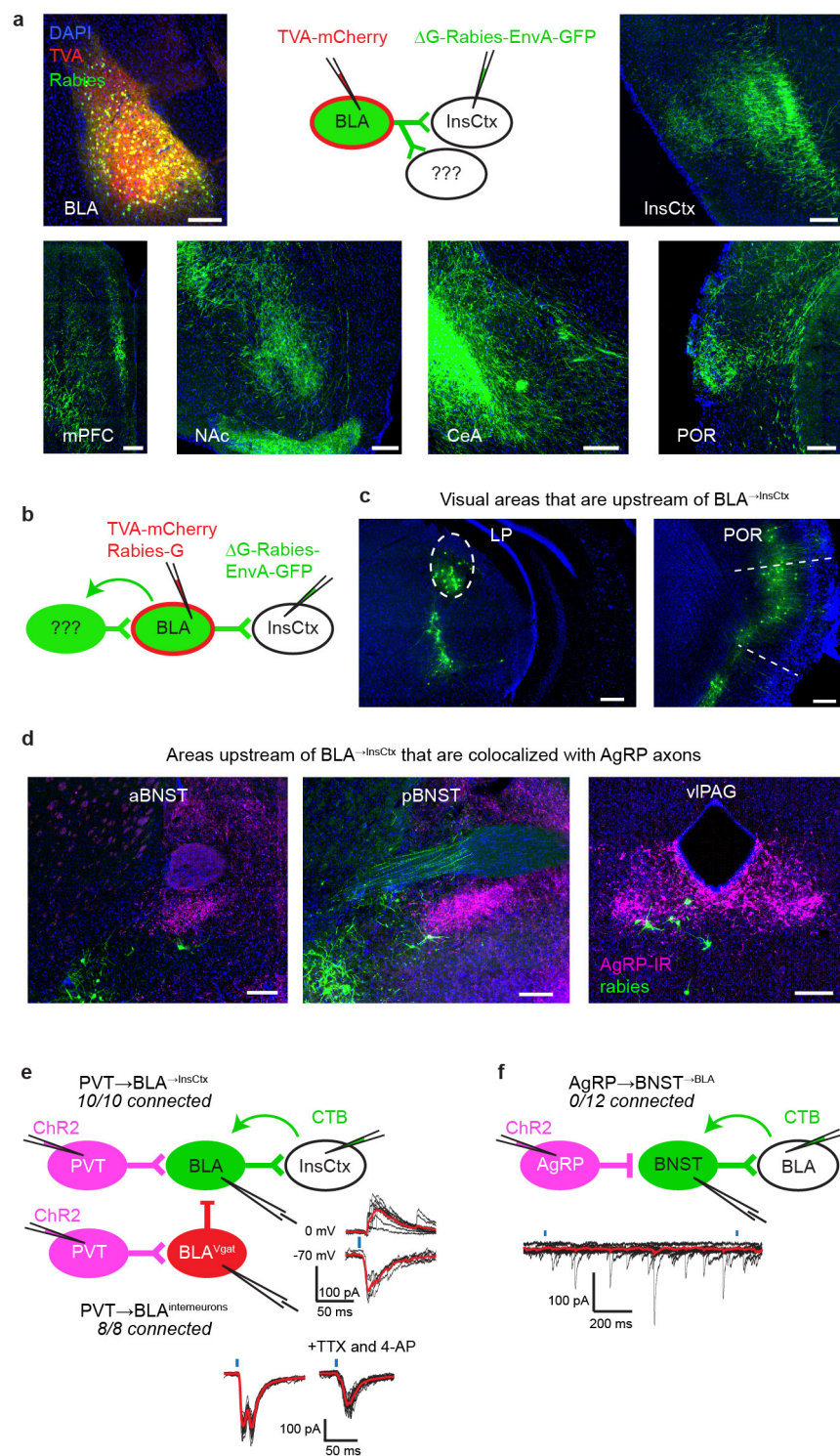
Extended Data Figure 8 | See next page for caption.

Extended Data Figure 8 | Further interrogation of the pathway from AgRP neurons to InsCtx. a, BLA$^{\rightarrow \text{InsCtx}}$ neurons send axon collaterals to several other BLA targets. Top middle: rabies-based axon collateral mapping approach. Top left: image of the BLA (AAV-FLEX-TVA–mCherry injection site in Emx1-ires-Cre mice), containing neurons labelled with TVA–mCherry (red) and rabies (green). Top right: image of InsCtx (rabies injection site) containing axons labelled with rabies (green). Bottom: images of additional sites that also contained axons labelled with rabies after rabies injection into InsCtx. Scale bars, 200 μm. mPFC, medial prefrontal cortex. **b–d**, Additional inputs to BLA$^{\rightarrow \text{InsCtx}}$. **b**, Schematic of rabies-based, projection-specific monosynaptic tracing of inputs to BLA$^{\rightarrow \text{InsCtx}}$ neurons. **c**, Images of visual areas containing rabies-labelled neurons (green). Scale bars, 200 μm. **d**, Images of additional sites containing rabies-labelled neurons (green) that anatomically co-localized with AgRP axons (magenta). vlPAG, ventrolateral periaqueductal grey; aBNST and pBNST, anterior and posterior bed nucleus of the stria terminalis, respectively. **e**, PVT neurons provide input to BLA$^{\rightarrow \text{InsCtx}}$ neurons and to BLA inhibitory interneurons. Left: schematic of CRACM from PVT neurons to BLA$^{\rightarrow \text{InsCtx}}$ neurons (labelled

by CTB injection in InsCtx) or to BLA inhibitory interneurons (labelled by AAV-FLEX–mCherry injection into BLA of Vgat-ires-Cre mice). Note that all recorded neurons received input from PVT (ten out of ten BLA$^{\rightarrow \text{InsCtx}}$ neurons, eight out of eight BLA inhibitory interneurons). Top right: light-evoked excitatory postsynaptic currents (−70 mV holding potential) and inhibitory postsynaptic currents (0 mV holding potential) in a BLA$^{\rightarrow \text{InsCtx}}$ neuron. Note the longer latency and higher temporal jitter of the inhibitory postsynaptic currents, suggesting that they were di/polysynaptic. Bottom right: light-evoked excitatory postsynaptic currents in a BLA interneuron. Note that light-evoked currents had two peaks (monosynaptic and di/polysynaptic), and that the second peak was eliminated by bath application of tetrodotoxin (TTX) and 4-aminopyridine (4-AP), demonstrating that it was di/polysynaptic. Scale bars, 100 pA, 50 ms. **f**, BNST$^{\rightarrow \text{BLA}}$ neurons did not receive monosynaptic input from AgRP neurons. Top: schematic of CRACM from AgRP neurons to BNST$^{\rightarrow \text{BLA}}$ neurons. Bottom: example recording of AgRP inputs to a BNST$^{\rightarrow \text{BLA}}$ neuron. Black lines are individual sweeps; red line is the average of 15 sweeps. No recorded BNST$^{\rightarrow \text{BLA}}$ neuron received input from AgRP neurons (0 out of 12 connected).
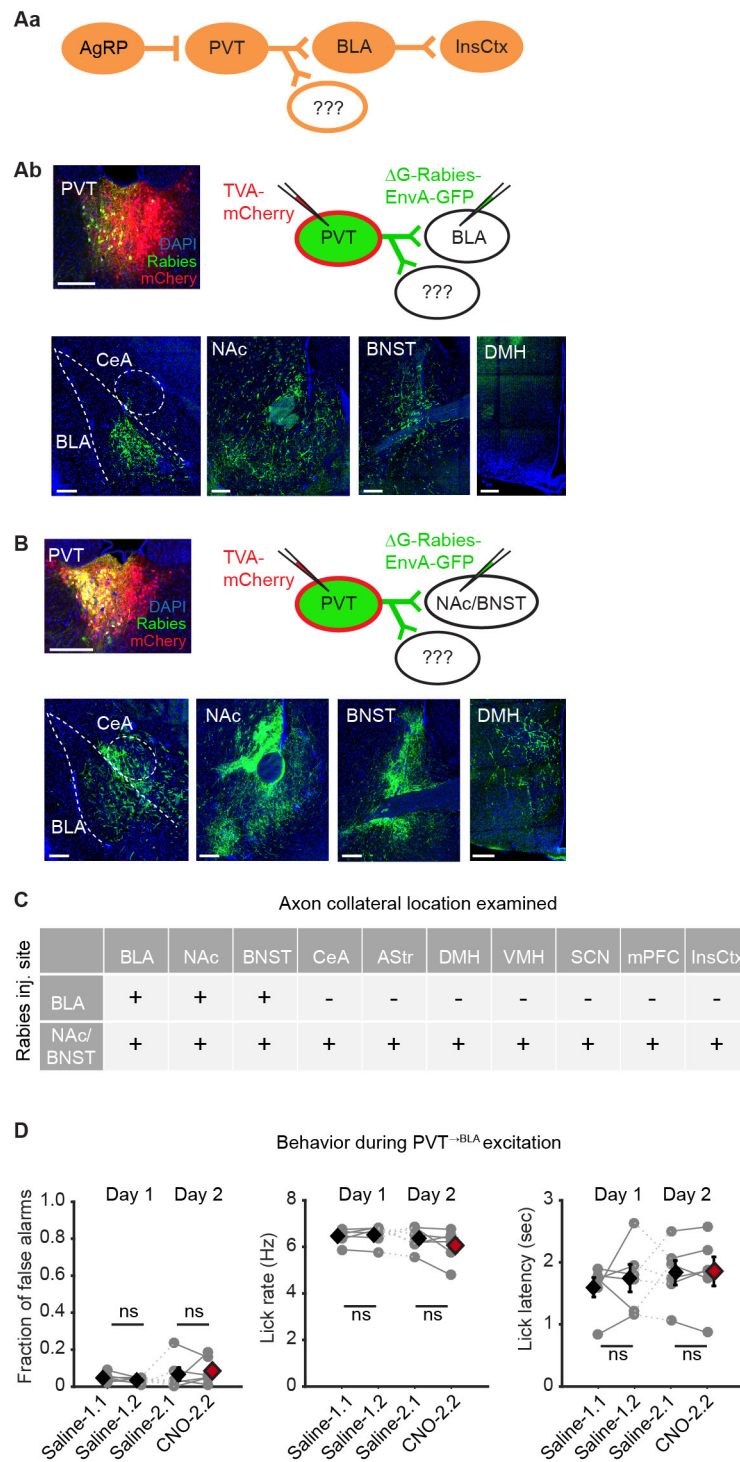
Extended Data Figure 9 | PVT$^{\rightarrow BLA}$ and PVT$^{\rightarrow NAc/BNST}$ collateral mapping; further behavioural analyses of PVT$^{\rightarrow BLA}$ excitation.
A–C, PVT$^{\rightarrow BLA}$ and PVT$^{\rightarrow NAc/BNST}$ collateral mapping. **A, a**, Summary of the proposed pathway from AgRP neurons to InsCtx, raising the question of whether PVT$^{\rightarrow BLA}$ neurons also project to other sites. Scale bars, 200 μm. **A, b**, PVT$^{\rightarrow BLA}$ neurons also project to NAc/BNST, but not to any other sites. Top right: rabies-based axon collateral mapping approach. Top left: image of the PVT (TVA–mCherry injection site) containing neurons labelled with TVA–mCherry (red) and rabies (green). Bottom: images of sites examined for the presence of labelled axons. Note that labelled axons were found in BLA (rabies injection site) and NAc/BNST, but not in CeA or dorsomedial hypothalamus (DMH). Scale bars, 200 μm. **B**, PVT$^{\rightarrow NAc/BNST}$ neurons sent collaterals to all PVT projection sites examined. Top right: rabies-based axon collateral mapping approach. Top left: image of the PVT (TVA–mCherry injection site) containing neurons labelled with TVA–mCherry (red) and rabies (green). Bottom: images of sites examined for the presence of labelled axons. Note that labelled axons were found in all sites examined. **C**, Summary of experiments in **A** and **B**. PVT$^{\rightarrow NAc/BNST}$ projected to all PVT projection sites examined, while PVT$^{\rightarrow BLA}$ only projected to BLA and NAc/BNST, but not to other sites. AStr, amygdalo-striatal transition area; VMH, ventromedial hypothalamus; SCN: suprachiasmatic nucleus. **D**, Further behavioural analyses of PVT$^{\rightarrow BLA}$ activation. Fraction of false alarms (left), lick rate (middle), and lick latency (right). Each dot represents one mouse; lines connect two same-day blocks from the same mouse (two saline blocks on day 1: Saline-1.1, Saline-1.2; and a saline block followed by a CNO block on day 2: Saline-2.1, CNO-2.2). Notice no significant changes on either day. Diamonds and error bars, mean ± s.e.m.; NS, not significant ($P \geq 0.2$); $n = 6$ mice.
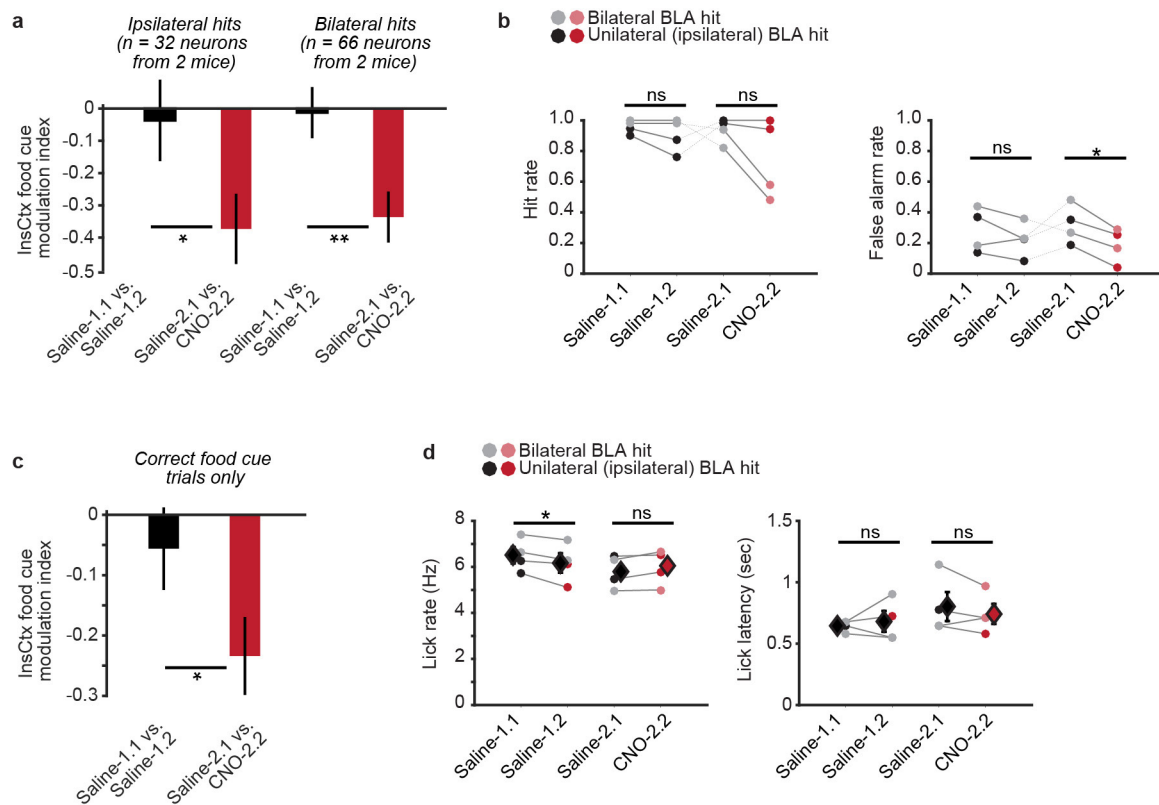
Extended Data Figure 10 | Further analyses of BLA$^{\rightarrow\text{InsCtx}}$ inhibition.
a, InsCtx food cue modulation index (in the absence versus presence of BLA$^{\rightarrow\text{InsCtx}}$ inhibition) for mice with ipsilateral (left) and bilateral (right) BLA hits. Note overall stability on day 1 (saline versus saline) but attenuation of cue responses (resulting in a negative food cue modulation index) after CNO injection on day 2 in both groups. Values are median ± s.e. median. *$P < 0.01$; **$P < 0.001$; Mann–Whitney U-test (ipsilateral: $n = 32$ neurons from two mice; bilateral: $n = 66$ neurons from two other mice). **b**, Behavioural responses to the food cue (left) and to the other cues (right) during BLA$^{\rightarrow\text{InsCtx}}$ inhibition. Each dot represents one mouse; lines connect two same-day blocks from the same mouse (two saline blocks on day 1: Saline-1.1, Saline-1.2; and a saline block followed by a CNO block on day 2: Saline-2.1, CNO-2.2). Dark dots: mice with ipsilateral (to InsCtx imaging hemisphere) hits; light dots: mice with bilateral hits. Note that behavioural responses to the food cue were reduced after BLA$^{\rightarrow\text{InsCtx}}$ inhibition only in the two

mice with bilateral hits, but that false alarm rates were reduced in all mice. *$P < 0.01$; NS, not significant ($P > 0.2$); paired t-test ($n = 4$ mice). **c**, InsCtx food cue modulation index calculated using only those trials with correct behavioural responses. Note overall stability on day 1 but attenuation of cue responses after CNO injection on day 2. Values are median ± s.e. median. *$P < 0.03$, Mann–Whitney U-test ($n = 98$ neurons from four mice). **d**, Lick rate (left) and lick latency (right) during BLA$^{\rightarrow\text{InsCtx}}$ inhibition. Each dot represents one mouse; lines connect two same-day blocks from the same mouse (two saline blocks on day 1: Saline-1.1, Saline-1.2; and a saline block followed by a CNO block on day 2: Saline-2.1, CNO-2.2). Note that lick rates exhibited a small but significant decrease between Saline-1.1 and Saline-1.2 (*$P = 0.04$), but no significant change between Saline-2.1 and CNO-2.2 ($P = 0.3$). There was no significant change in lick latency ($P > 0.3$). NS, not significant; paired t-test ($n = 4$ mice).